



Sedimentary architecture of the Brown Bank Formation (Dutch sector of the North Sea) reveals consecutive shallow marine depositional phases during the MIS 5-4 transition

Irene Waajen-Labee^{a,b,*}, Ruth Plets^c, Víctor Cartelle^c, Marieke Cuperus^a, Timme Donders^a, Sytze van Heteren^b, Thomas Mestdag^c, Friederike Wagner-Cremer^a, Jakob Wallinga^e, Frank Wesselingh^{d,a}, Freek Busschers^b

^a Faculty of Geosciences, Utrecht University, Utrecht, the Netherlands

^b TNO – Geological Survey of the Netherlands, Utrecht, the Netherlands

^c Flanders Marine Institute (VLIZ), Oostende, Belgium

^d Naturalis Biodiversity Center, Leiden, the Netherlands

^e Soil Geography and Landscape Group & Netherlands Centre for Luminescence Dating, Wageningen University, Wageningen, the Netherlands

ARTICLE INFO

Keywords:

North Sea
Glacial inception
Seismostratigraphy
Biostratigraphy
Palaeoenvironment
Brown Bank

ABSTRACT

Major climate cooling transitions have large impacts on the evolution of sedimentary depositional systems of shelf seas and coastal areas. These transitions are rarely preserved because they are prone to erosion during subsequent lowstands or, if preserved, buried too deep to reach with standard ground-truthing methods. As result, the relation between climate cooling and these sedimentary systems is still poorly understood. Severe climate cooling occurred during the Late Pleistocene MIS 5-MIS 4 transition, as captured within the shallow marine deposits of the Brown Bank Formation (Fm), which occurs between 0.1 m and 40 m below the present southern North Sea floor. To improve our understanding of the character and complexity of the depositional system, as well as the environmental response during the rapid climate cooling it portrays, we map the hitherto poorly constrained extent and architecture of the Brown Bank Fm within part of the Dutch sector of the North Sea. We document and map four seismic facies units (BB1-BB4) that are attributed to variations in tidal energy and pro-deltaic sediment supply. Pollen, diatom and mollusc assemblages reveal that the palaeoenvironment remained shallow marine throughout deposition and provide evidence for two cooling phases. The pollen assemblage also indicates that during this period forests changed to open woodlands in this period. Linking the palaeoenvironmental data and new luminescence ages of the four units with the Greenland NGRIP $\delta^{18}\text{O}_{\text{ice}}$ chronology, suggests that deposition of the units occurred during a relatively short time. The new analyses from the Brown Bank Fm suggest that the North Sea became disconnected from the Atlantic Ocean at its southern outlet (the Dover Strait) around the start of MIS 5a (ca. 88 ka) and that the floor of the southern North Sea became completely exposed around 72 ka.

1. Introduction

Coastal and shallow marine depositional systems were significantly influenced by Quaternary climate fluctuations (Busschers et al., 2007; Eaton et al., 2020; Hijma et al., 2012; Schimanski and Stattegger, 2005; Shennan et al., 2000). Sea-level variations during glacial-interglacial transitions, as well as during shorter stadial-interstadial intervals

(Gowan et al., 2021; Spratt and Lisiecki, 2016), triggered strong and rapid coastline shifts and the emergence and disappearance of deltas and estuaries. Sedimentary depositional records that formed under falling sea-level conditions (the falling stage systems tracts; Catuneanu, 2022) are not always recognized and are rarely preserved on continental shelves due to subsequent erosion during glacial lowstands or during marine transgressions (Cattaneo and Steel, 2003). Where marine

Abbreviations: MIS, marine isotope stage; LAT, lowest astronomical tide; TWT, two-way travel time; GIS, Greenland interstadial; GS, Greenland stadial; IJW, IJmuiden Ver Windfarm zone; HKW, Hollandse Kust West windfarm zone; bsf, below sea floor.

* Corresponding author. Faculty of Geosciences, Utrecht University, Utrecht, the Netherlands

E-mail address: irene.waajen@tno.nl (I. Waajen-Labee).

<https://doi.org/10.1016/j.quascirev.2025.109442>

Received 17 January 2025; Received in revised form 9 May 2025; Accepted 21 May 2025

Available online 27 June 2025

0277-3791/© 2025 The Authors. Published by Elsevier Ltd. This is an open access article under the CC BY license (<http://creativecommons.org/licenses/by/4.0/>).

sedimentary records of falling sea-level conditions are preserved, the offshore location of such deposits and their subsequent burial often complicates their sampling and study.

The MIS 5-MIS 4 transition (ca. 80-70 ka) is such a period characterised by strong global sea-level lowering and severe climate cooling (De Clercq et al., 2018; Huijzer and Vandenberghe, 1998; Spratt and Lisiecki, 2016). Within the British and Dutch sectors of southern North Sea (Fig. 1a), a key sedimentary unit linked to this period has been well-preserved and, crucially, is within easy sampling reach. This unit, known as the Brown Bank Formation (Fm) is typically recognized on seismic survey data as having a distinct parallel reflection configuration (e.g. Cameron et al., 1989). In boreholes, the sediments are seen to mainly consist of bioturbated silty clays (Cameron et al., 1989; Waajen et al., 2024a; Waajen et al., 2024b). North of the area where the Brown Bank Fm deposits occur, potential deposits from the same time period may have been removed by subsequent glacial erosion, whilst further south it was either never deposited or not preserved. The Brown Bank Fm deposits have been interpreted in earlier studies to reflect a mainly brackish to fresh-water environment during the onset of the Early Weichselian (pollen zone EW1; Zagwijn, 1983), whilst other studies show marine conditions (Cameron et al., 1992; Oele, 1971), and more recently a younger age (85-50 ka; Limpenny et al., 2011; Wessex Archaeology, 2018) was proposed based on optically stimulated luminescence (OSL) dating (Waajen et al., 2024a; Wessex Archaeology, 2018). The latest results from the Dutch sector indicate that the Brown Bank Fm represents low energy, shallow marine, cool to very cold depositional settings (Waajen et al., 2024b). It is currently unknown

how long the southern North Sea remained a marine basin, if it evolved towards a brackish or freshwater basin, and when it became (partially) dry land. The Brown Bank Fm is generally described as a single unit, but more recently, it has been subdivided into an upper and lower unit (Eaton et al., 2020; Wessex Archaeology, 2018). So far, the Brown Bank Fm has mainly been studied by either focusing on short sediment cores (Cameron et al., 1989; Waajen et al., 2024a; Waajen et al., 2024b) or seismic surveys (Eaton et al., 2020), but regional correlations combining seismic surveys with high-resolution proxy data from multiple cores have only been applied sparsely, mainly for the archaeological assessment of wind farm areas (e.g. Waajen et al., 2024a; Periplus Archaeomare, 2023; 2023b). Deposits of the Brown Bank Fm can provide new insights into the environmental and sea-level responses to the rapid climate change of the MIS 5-4 transition. Cooling at the last interglacial-glacial transition (MIS 5a – 4 transition) has been shown to include complex climate variations with alternating short but severe stadial and interstadial phases (Sánchez Goni et al., 2013). However, the stratigraphic record of the associated alternating sea-level rises and falls in this overall falling stage systems tract remains understudied. Constraining the rate of climate and sea-level change and the response of depositional environments during glacial inception is crucial for global and regional sea-level reconstructions and ground-truthing sea-level models (e.g. Gowan et al., 2021; Toucanne et al., 2023). Therefore, the aim of this study is to examine the Brown Bank Fm in detail to better understand (1) the response of the coastal architecture and shallow marine environments and (2) the exact timing of these changes, during this period of global climate cooling.

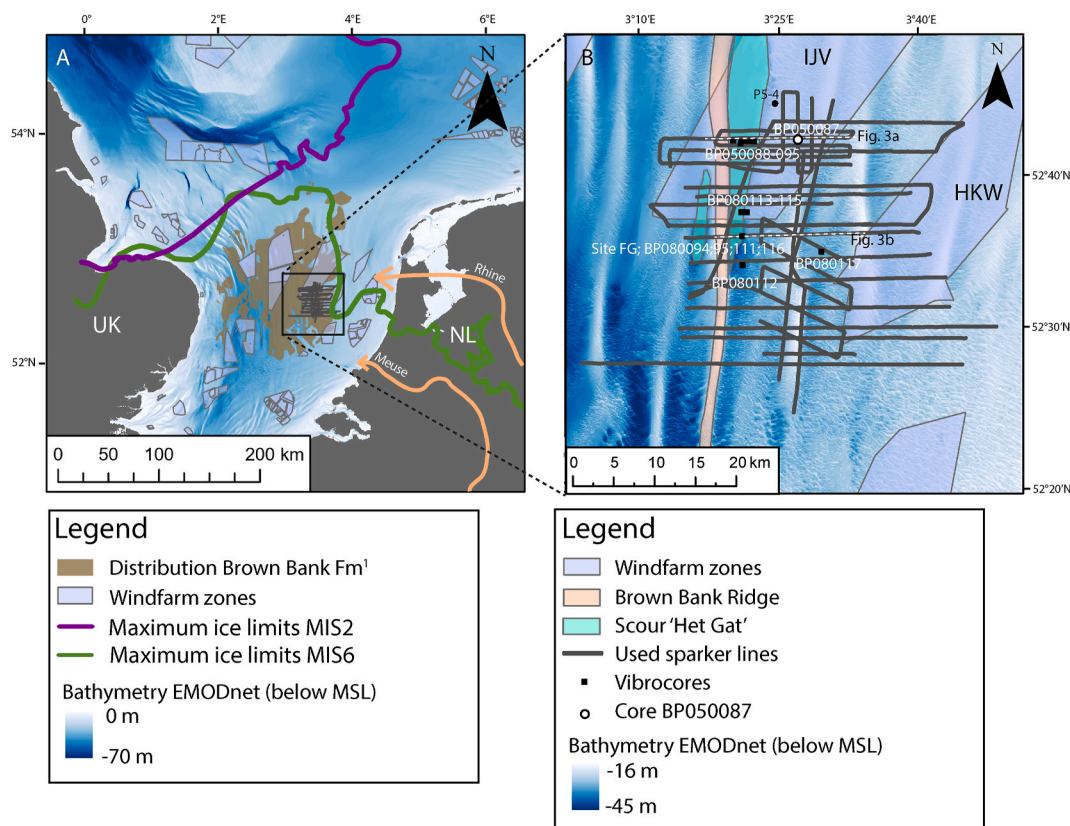


Fig. 1. a) bathymetric map of the southern North Sea (EMODnet Bathymetry Consortium, 2020) including wind farm zones (EMODnet, 2022) and the distribution of the Brown Bank Fm (Cameron et al., 1989). The maximum ice extents are shown for MIS 6 (Saalian, Drenthe glaciation; based on Batchelor et al., 2019; Hijma et al., 2012; Joon et al., 1990; Moreau et al., 2012) and MIS 2 (Weichselian; based on Batchelor et al., 2019; Hijma et al., 2012). The courses of the Rhine and Meuse rivers during the Early Weichselian are indicated in orange, with the arrow pointing towards the approximate location of their delta, based on (Hijma et al., 2012; Peeters et al., 2015). b) Detailed bathymetry map of the study area. The location of the Brown Bank Ridge and 'Het Gat' (also used in Figs. 2 and 4) are shown. The Sparker seismic reflection lines used in this study are shown and the locations of the profiles in Fig. 3 are indicated with white dotted lines labelled 3a and 3b, along with the cores used for this study. Wind farm zones IJmuiden Ver (IJV) and Hollandse Kust West (HKW), both in the Dutch sector of the North Sea, are annotated. (For interpretation of the references to colour in this figure legend, the reader is referred to the Web version of this article.)

Specifically, this study presents a detailed stratigraphic framework for the Brown Bank Fm based on a high-density grid of seismic reflection profiles and multiple cores with lithological characterisation. Subsequently, this stratigraphic framework is combined with OSL dates and biological proxies (pollen, mollusc and diatom assemblages) focusing on a deep drill core through the Brown Bank Fm (core BP050087), which sheds light on the complexity of that unit. This work builds on previous research of the Brown Bank Fm at the flank of the Brown Bank ridge, named 'Het Gat' (site FG in Waajen et al., 2024a; Waajen et al., 2024b) and expands to a larger region, providing more regional-scale insights into the shallow marine system. A new (seismo)stratigraphic framework combined with multi-proxy environmental data enables the reconstruction of the shallow marine palaeolandscape and ecosystem development during this period of falling sea level and climate cooling. The new palaeoenvironmental framework is subsequently used to augment existing palaeogeographic reconstructions of the fluvial and coastal configuration of the southern North Sea region during MIS 5 and MIS 4 (Busschers et al., 2007; Hijma et al., 2012; Peeters et al., 2015).

2. Setting and study area

The southern North Sea is a shallow shelf sea where the Quaternary sedimentary successions are strongly influenced by glacial and interglacial cycles (Cameron et al., 1992; Hijma et al., 2012; Jansen et al., 1979). Sea-level fluctuations resulted in periods of alternating shelf submergence and exposure, which resulted in a complex stratigraphic record (Cameron et al., 1989; Eaton et al., 2020; Emery et al., 2019a; Head and Gibbard, 2015; Hijma et al., 2012). Our understanding so far of the offshore Quaternary stratigraphy is seismostratigraphic in nature, supplemented with limited borehole information (Cameron et al., 1989; Eaton et al., 2020). In contrast, our knowledge of the onshore stratigraphy is based on a combination of borehole data, geophysical data and various other sources (Ten Veen et al., 2025). In the past decade, the development of offshore wind farms (Fig. 1a) increased the amount of offshore seismic and borehole data from the North Sea considerably, offering opportunities to expand our knowledge of the offshore record in this area (e.g. Cartelle et al., 2021; Eaton et al., 2020; Emery et al., 2019b; Velenturf et al., 2021).

Our study area is located in the central part of the southern North Sea, on the south-east side of the mapped distribution of the Brown Bank Fm (Cameron et al., 1989, Fig. 1b). The study area is ca. 35 × 35 km, which is large enough to see the regional stratigraphic architecture, but small enough to be able to analyse the complexity of the subsurface. The sea floor in the study area is currently between 15 and 46 m below mean sea level (MSL), and the bathymetry is dominated by a ridge and swale morphology, with three N-S oriented sand banks. The most prominent high has been labelled as Brown Bank Ridge, on navigational charts annotated as the Brown Ridge, located within the wider Brown Bank area (Fig. 1b). Within the swales, Holocene deposits are thinnest. In the deepest swale, directly east of Brown Bank Ridge and named 'Het Gat' (Fig. 1b), deposits of the Middle Pleistocene Yarmouth Roads Fm and Late Pleistocene Brown Bank Fm are present directly below the sea floor (Waajen et al., 2024a).

The study area is located on the southern shoulder of the North Sea Basin (Kooi et al., 1998; Lamb et al., 2018) with average subsidence rates (for the last 1.8 Ma) of 0.06–0.14 m/kyr, based on the depth of the base of the Pleistocene in marine formations (Cohen et al., 2022). Depending on the position within the study area, this is equivalent to a total of 4.5–10.5 m during the last 75 kyr (Cohen et al., 2022). The southern North Sea is a unique location for studying palaeoenvironmental evolution as it is influenced by both terrestrial and (shallow) marine processes (Waajen et al., 2024a; Waajen et al., 2024b), with high accumulation rates resulting in high-resolution sedimentary records. The Rhine was the largest river that deposited sediments in the study area, with the MIS 5 Rhine delta being located in the northern part of the Netherlands, almost 100 km farther north than at present. Besides

the Rhine, the Meuse, Thames and Scheldt rivers also discharged into the area but had less direct influence on deposition (Hijma et al., 2012; Peeters et al., 2015).

3. Methods

3.1. Seismic reflection data

Seismic reflection (Sparker) surveys were conducted in the study area between 2018 and 2022. The data presented here were collected during three scientific surveys onboard the RV *Simon Stevin*: June 2021 (SS2021/470), 2022 (SS2022/230) and 2023 (SS2023/490). Depending on equipment and deck space availability, different Sparker systems were deployed during different surveys. More specifically, in 2021, data were acquired with a GSO360 high-resolution multi-tip Sparker source (centre frequency of 800 Hz, deployed at 800 J, ping rate of 0.5 s) along with a SIG multi-channel streamer (consisting of 24 channels at 2 m spacing). In 2022, the GSO360 system was deployed with a SIG single-channel streamer. During the 2023 survey, a multi-tip Centipede source (centre frequency of 1.1–1.2 kHz, deployed at 400 J, ping rate of 0.5 s) along with a SIG dual-channel streamer was used. Data were recorded using a Delph analogue acquisition system with a sampling frequency of 8 kHz (2021) and 16 kHz (2022, 2023). The Sparker source and streamer were towed 35 m behind the vessel from the port and starboard side, respectively. Whilst the data were recorded to a depth of 300 ms (ca. 225 m), the imaging quality is best within the top 100 m, with a vertical resolution of 0.5–1.5 m. Given a vessel speed of 3–4 kn during acquisition, the along-track sampling distance is ca. 1 m.

Processing of the seismic reflection data was performed in RadExPro, which for the single- and dual-channel data (2022, 2023) consisted of geometry assignment, amplitude corrections, filtering (bandpass filter, swell filter, burst noise removal and 2D spatial filter), wavelet deconvolution and tidal corrections (to lowest astronomical tide, LAT). Processing of the multi-channel data (2021) encompassed geometry definition and binning, swell filtering, wavelet deconvolution and receiver deghosting in the pre-stack phase. A velocity model was then generated per profile by manually picking normal move-out (NMO) velocities in the common depth point gathers, which was subsequently used to perform the NMO correction and stacking. Finally, in the post-stack phase, Kirchhoff time migration, an additional wavelet deconvolution, 2D spatial filtering and tidal corrections (to LAT) were applied.

All processed Sparker profiles were imported into S&P Global Kingdom software for interpretation, visualisation, correlation with the core data and gridding. The seismic survey lines were used to identify seismic facies and seismostratigraphic units. The characterisation of the seismic units and facies was performed following the standard principles of seismic stratigraphy (Mitchum et al., 1977; Mitchum and Vail, 1977), examining seismic reflection characteristics and terminations, bounding surfaces, as well as larger geomorphological structures (e.g. incisions, depressions, ridges). For this study, the analyses and interpretation of the seismic profiles focused on mapping sub-units within the Brown Bank Fm, and, for simplicity, younger and older units were considered to correspond to pre- and post-Brown Bank Fm, respectively. A conversion from two-way travel time (TWT) to depth (m) was applied using a sound velocity of 1550 m/s in water and 1650 m/s in sediments. This interval velocity was based on the best-fit correlation between the seismic profile TNO_BP050087_01, acquired in 2023, and borehole BP050087. Such depth conversion was used to create gridded thickness and bounding surface distribution maps. To create these grids, a flex gridding algorithm was used with a grid cell size of 500 m and limiting the distance from the control point to 500 m from an input datapoint. These grids were subsequently exported to a GIS environment for further interpretation.

3.2. Sediment cores

3.2.1. Core collection

During multiple cruises, 18 sediment cores were obtained in the study area. Cores BP080117, BP080111 (VC34, Waajen et al., 2024a; 2024b), BP080094 (VC35, Waajen et al., 2024a; 2024b) and BP080095 (VC36, Waajen et al., 2024a; 2024b) were collected onboard the RV *Pelagia* (cruise 64PE439) in July 2018 using a Marine Sampling Holland electrical vibrocorer with a maximum core retrieval of 5 m. Water depth was determined relative to MSL based on a multibeam echosounder on board RV *Pelagia* and corrected for the tides. The largest set of cores used for this study was collected onboard the RV *Simon Stevin* in 2022 (cruise SS2022/320). These are cores BP050088, BP050089, BP050090, BP080112, BP050091, BP050092, BP050093, BP050094, BP050095, BP080113, BP080114, BP080115 and BP080116. These cores were collected using an OSIL high-power vibrocorer system with a maximum core retrieval of 3 m. The longest core used for this study, is core BP050087 taken with a WISON MKV ECODRIVE sampling system, onboard the *Fugro Quest* in December 2022. Core sections were taken in steps of 1 m to a total depth of 20.25 m below the sea floor (m bsf). Table 1 provides the metadata of the cores, simplified logs are presented in Fig. S1 (except for BP050087, which is presented in Figs. 6–8, and a core photograph in Fig. S4), and core photos can be viewed in the DINOLoket database (www.dinoloket.nl/en) of the Geological Survey of the Netherlands (GSN).

3.2.2. Sedimentary facies

The sediment succession of each core was logged, focusing on the grain size, grain shape, colour, bioturbation, abundance of shells and gravel, and sedimentary structures. Simplified core logs are provided in Fig. S1. The cores from cruise 64PE439, as well as core BP050087, were logged by the Geological Survey of the Netherlands (GSN), while the SS22-320 cores were split, photographed, described and logged at the Flanders Marine Institute (VLIZ). Based on all core logs, lithofacies were defined and characterised.

3.3. Palaeoenvironmental analyses and dating

3.3.1. Pollen (BP050087)

Palynological analyses of pollen and spores provide information on the vegetation dynamics and past climate dynamics on the land surrounding the southern North Sea. As the palynomorphs are transported from land to the North Sea, the composition carries an imprint of the transport process. Pollen analyses is used as a (biochronological) correlation tool (Cain, 1939; Seppä and Bennett, 2003) where comparison

to pollen zones in other sites provides biochronological constraints on the period of deposition. For pollen analyses, 49 sediment samples were taken from core BP050087 using a 1 cm³-sampler, except for 4 samples which targeted thin laminae, where $\frac{2}{3}$ cm³ was sampled. First, *Lycopodium* marker spores (ca. 3971 per sample) were added to allow the calculation of pollen concentration. Subsequently, these samples were processed for pollen analysis following Faegri et al. (1989). In summary, 5 % HCl was used for carbonate removal, followed by 5 % KOH treatment of 60 min at 70 °C to remove humic material. Sieving with 6 µm and 120 µm mesh captured the size fraction of pollen. Subsequently, acetolysis (acetic anhydride and sulphuric acid, 9:1 v/v) of 5 min at 100 °C was used to dissolve polysaccharides and enhance contrast. After density separation of the pollen residues from mineral fractions by sodium polytungstate at a density of 2.0 g/cm³, the pollen residues were mounted in glycerol on glass slides. For each sample at least 200 pollen were counted, unless <200 were present in a sample, using a Leica DMLB optical microscope with 400x magnification. Counts were cross checked between analysts, and corrected where necessary. Spores, freshwater algae (*Pediastrum* and *Botryococcus*), dinoflagellate cysts and organic foraminifera linings were also counted. All tree, shrub, upland herb and heath pollen are included in the pollen sum, similar to the record of core BP080094 in Waajen et al. (2024a).

3.3.2. Diatoms (BP050087)

The composition of diatom assemblages depends on many physical and biochemical factors, such as salinity, pH, nutrients, temperature, turbidity, and current velocity. The diatom assemblages are used for reconstructing paleoenvironmental changes (Barlow et al., 2013; Vos and de Wolf, 1993) including changes in salinity and indications for water depth. For diatom analyses, the mineral residues from 40 pollen samples in core BP050087 were treated with heavy liquid floatation using sodium polytungstate at a density of 2.3 g/cm³. Samples were cleaned with HCl and cold H₂O₂ to remove the carbonates and oxidise the organics, respectively (Cvetkoska et al., 2012). Of these 40 samples, 34 contain at least some diatoms. Permanent diatom slides were made using Zyrax as mounting medium. At least 200 diatoms were counted at each slide, except for samples with low diatom abundance where 200 was not reached, using the linear counting method under 1000x magnification with an Olympus BX51 microscope. Diatoms species identification followed Witkowski et al. (2000) and Krammer & Lange-Bertalot (1986–1991) and standard available diatom literature. Nomenclature follows the ‘Taxa Waterbeheer Nederland’ (TWN) list, while ecological groups according to species salinity preferences and life forms are based on the classification of Vos and de Wolf (1993). Zonation was determined using a constrained incremental sum of squares

Table 1

Metadata of all cores used for this study. Cruise numbers are related to the research vessels, where PH462 belongs to RV *Fugro Quest*, SS22_320 to RV *Simon Stevin*, and 64PE439 to RV *Pelagia*.

Core number (GSN)	Working name core	Cruise number	Date drilled	Latitude	Longitude	Core length (m)	Sea floor depth (m-MSL)
BP050087	BBQ	PH462	20/12/22	3.453496	52.70933	20.25	29.5
BP050088	VC08	SS22_320	12/06/22	3.336064302	52.70672613	2.165	42.2
BP050089	VC09	SS22_320	12/06/22	3.350728863	52.7059548	2.46	43.2
BP050090	VC10	SS22_320	12/06/22	3.349530647	52.70330431	1.43	43.4
BP080112	VC12_2	SS22_320	14/06/22	3.3523574	52.5693556	1.04	37.4
BP050091	VC13	SS22_320	12/06/22	3.356819029	52.70601846	2.545	44.3
BP050092	VC14	SS22_320	12/06/22	3.35766505	52.70599388	2.33	44.2
BP050093	VC15	SS22_320	12/06/22	3.363852399	52.70596844	0.755	42.2
BP050094	VC16	SS22_320	12/06/22	3.369688775	52.70589764	2.00	40.1
BP050095	VC17	SS22_320	12/06/22	3.373786967	52.70582508	2.605	37.6
BP080113	VC21	SS22_320	14/06/22	3.3517246	52.6278976	1.30	39.4
BP080114	VC22_2	SS22_320	14/06/22	3.3524069	52.6278813	1.645	35.6
BP080115	VC23	SS22_320	14/06/22	3.3602984	52.6275205	2.375	34.0
BP080116	VC24	SS22_320	14/06/22	3.3521096	52.6014962	1.76	37.4
BP080117	VC33	64PE439	24/06/18	3.503217	52.584009	2.84	31.9
BP080111	VC34	64PE439	24/06/18	3.351043	52.601383	2.66	39.3
BP080094	VC35	64PE439	24/06/18	3.350908	52.601059	3.00	39.8
BP080095	VC36	64PE439	24/06/18	3.350775	52.601051	3.05	39.8

cluster analysis (CONISS; Grim 1987), using diatom taxa with abundances >2 %.

3.3.3. Molluscs (BP050087 and BP050094)

Mollusc shells can provide strong palaeoenvironmental insights, including information on energy, climate and water depth within a marine setting. Different mollusc assemblages are present in different climatic zones (e.g. boreal or arctic) and in different depositional settings (e.g. shoreface settings above storm-wave base compared to lower shoreface and upper shelf areas). For mollusc analysis, 49 and 7 sediment samples were taken from cores BP050087 and BP050094, respectively, covering an interval between 2 and 10 cm of one half of the split core. In addition, the coarse fraction (>250 µm) of the 12 sediment samples for OSL dating from core BP050087 were also analysed for shell fragments. The sediment samples were wet-sieved on a 0.5-mm mesh sediment sieve. The sedimentary residues were characterised. Mollusc shells and fragments were identified and classified as autochthonous or (para-)allochthonous based on preservation characteristics (*sensu* Kidwell, 1986), similar as in Waajen et al. (2024b).

3.3.4. X-ray fluorescence (XRF) core scanning (BP050087)

XRF core scanning is a fast and non-destructive method to assess the elemental composition in unprocessed core sediments. These elemental proxy data can reflect past climate, can provide detailed archives of the paleoenvironment and provide a tool for stratigraphic correlations (Hennekam and de Lange, 2012; Rothwell and Croudace, 2015). The general composition of the sediment can be analysed to observe changes in sediment source or depositional environment. XRF core scanning was performed on core BP050087 at NIOZ (Royal Netherlands Institute for Sea Research) with an Avaatech scanner with a similar procedure and settings as cores BP080094 and BP080095 described in Waajen et al. (2024a). In summary, the unsampled archive halves of the core were covered with a 4-µm SPEXCerti Ultralene foil, and then measured with a 10 mm step size using three energy settings (10 kV at 550 µA, 30 kV at 200 µA and 50 kV at 175 µA).

To statistically analyse the full variability of the XRF-dataset, the elemental data were first transformed using a centered log-ratio (clr) transformation, after which a hierarchical cluster analysis (HCA) was performed on the clr-normalised dataset (following Martin-Puertas et al., 2017; McGuire, 2020). HCA divides the dataset into compositional clusters with similar geochemical signatures, without prior knowledge. We applied HCA on the following elements: Al, Si, S, Cl, K, Ca, Ti, Cr, Mn, Fe, Cu, Zn, Br, Rb, Sr, Zr and Ba, and applied Ward's minimum variance method, aiming at finding spherical and compact clusters, using the option 'ward.D2' from function 'hclust' of the R package *stats* (version 4.2.2). The Euclidian linkage distances between the clusters provide information on the appropriate amount of clusters that best explain the variability within the dataset. The geochemical clusters were plotted against depth to guide the sedimentological zonation of the core, which provides a geochemical-based statistical sub-composition of the sediments.

3.3.5. Luminescence dating (BP050087 and BP080117)

Dating of the sediments is crucial for placing the sedimentary deposits in a frame of global climate trends. Luminescence dating is an absolute dating method which determines the timing of last light exposure, and thus the burial age, of sand-sized quartz and/or feldspar mineral grains. From core BP050087, twelve sediment samples were obtained in safe light conditions at GSN. These samples were analysed at the Netherlands Centre of Luminescence dating (NCL) for both quartz OSL and feldspar post-infrared infrared-stimulated luminescence (pIRIR) dating. In addition, eight sediment samples from core BP080117 were measured for luminescence dating at the School of Earth and Environmental Sciences (SEES), University of St Andrews, using only quartz OSL. Luminescence dating methods are not fully standardized between labs, and the NCL and SEES facilities operated independently

during this project, similar as described in Waajen et al. (2024a). This resulted in two different techniques (NCL vs. SEES) being applied for estimating the effective environmental dose rate, as well as three different approaches for the measurement and analysis of luminescence signals. A brief discussion on the challenges of comparing OSL dates from different labs can be found in Waajen et al. (2024a). Details on measurement protocols, age distributions and dose-response curves are provided in appendix A.

4. Results and interpretations

4.1. Seismic data

Traditionally, the Brown Bank Fm has been recognized on seismic reflection profiles as a regionally extensive amalgamated unit consisting of medium-to high-amplitude subparallel internal reflections, bounded by high-amplitude lower and upper bounding reflections. Our new data from the Brown Bank Fm reveal the occurrence of more transparent seismic facies together with the typical parallel reflections. The base of the formation can be traced as a continuous horizon (H1). It is undulating, with a general trend displaying a gentle dip from ca. −37 to −45 m LAT (locally deeper) in a north-westward direction over the length of the study area (ca. 35 km; Fig. 2a). In the southern central part of the area, H1 forms the base of an elongated N-S-oriented trough structure, with depths reaching up to −59 m LAT. The upper boundary (H5) is characterised as an almost continuous high-to medium-amplitude reflection, which truncates the underlying structures. Its depth varies between ca. −30 and −46 m LAT, forming distinct ridges and troughs (Fig. 2b). The thickness of the Brown Bank Fm usually does not exceed 5 m, but it can locally reach up to 20 m (Fig. 2c).

Further detailed analyses show four distinct seismic elements within the Brown Bank Fm (units BB1 to BB4) (Fig. 3). The characteristics of each of the units are summarised in Table 2, and can be described as follows, from bottom to top:

Unit BB1 is the lowermost unit, which is acoustically transparent and overlies the basal horizon H1 (Table 2). The transparent nature of the unit suggests that its lithology is fairly uniform, probably dominated by sand. Horizon H1 is slightly undulating, and unit BB1 is thinner within the depressions and thicker on their margins (Fig. 4). The top of the unit, horizon H2, is a medium-to high-amplitude wavy reflection. On seismic profiles, what remains of the unit is seen to form a set of low-mounded structures, or ridges, no thicker than 5 m and usually less than 3.5 m, separated by scour- or trough-like depressions (e.g. Fig. 3a at 6–10 km). On the gridded data (Fig. 4), unit BB1 appears to form an N-S-oriented complex of elongated structures up to 20 km in length and a few km in width in the northern and eastern parts of the study area. The upper horizon H2 displays a wavy appearance, indicative of migrating sandy bedforms on a scale matching present-day sand waves (Table 2). Unit BB1 only occurs in the northern part of the study area (Fig. 4).

Unit BB2 is also confined to the north of the study area, forming several N-S-oriented infill structures of up to 3 km in width (Figs. 4), 7.5m in thickness and occurring to a maximum depth of ca. −49 m LAT. At the base, the sides of these infill structures are constricted by unit BB1 (e.g. Fig. 3b at 13–19 km). The seismic facies of unit BB2 is dominated by continuous, medium-amplitude, medium-frequency reflections (Table 2) draping the underlying topography and infilling lows formed by H1 and H2. The parallel reflections are suggestive of an infill with stratified sediment. The BB2 infill is divergent with some onlap terminations on the sides. On the gridded data (Fig. 4), the N-S-oriented structures of this unit are curved and sinuous, and the remaining deposits of unit BB2 are confined to the scours or troughs formed during deposition of unit BB1. However, no clear gradient of the infill base can be derived from the available data. The top of the unit is clearly eroded by processes responsible for overlying horizons (H3, H4b and H5), indicating that the unit must have had a wider extent.

Unit BB3 can be traced adjacent to unit BB2, and mostly overlays unit

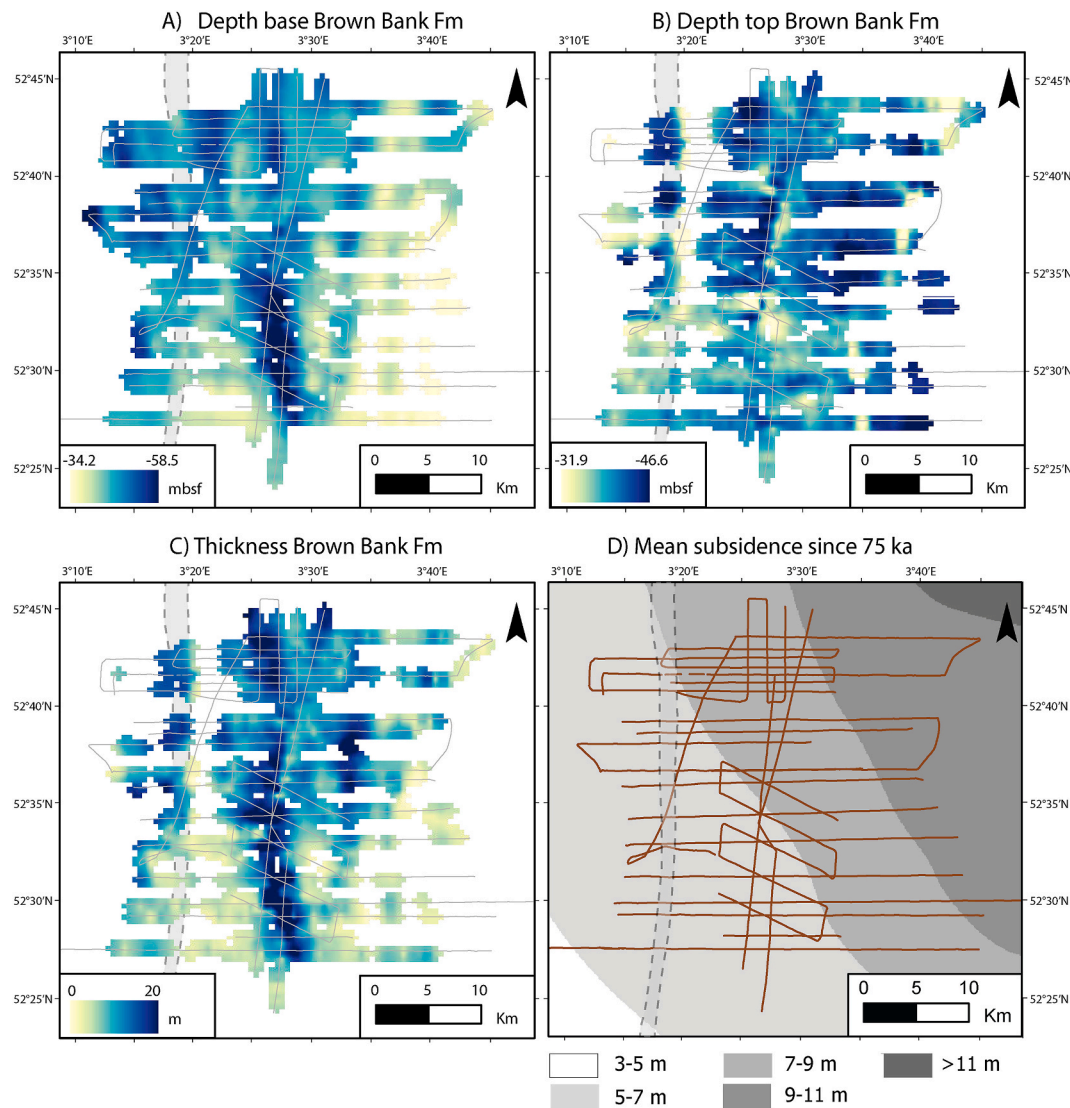


Fig. 2. Grids of the vertical range and thickness of the Brown Bank Formation. The location of the grid is shown in Fig. 1b and the location of the Brown Bank Ridge is included for reference as a grey vertical band. A) depth below LAT of horizon H1, representing the base of the Brown Bank Fm; B) depth below LAT of horizon H5, representing the top of the BB Fm; C) vertical distance between H1 and H5, representing the thickness of the entire BB Fm; D) average background subsidence over the past 75 ka, based on average subsidence rates provided by Cohen et al. (2022). (For interpretation of the references to colour in this figure legend, the reader is referred to the Web version of this article.)

BB1. It is seen in the seismic profiles as a lens-shaped unit (e.g. Fig. 3a from 6 to 11 km). The seismic facies is mostly transparent at the base, becoming chaotic towards the top (Table 2). Near the top, some reflections resembling (climbing) sediment waves can be discerned, indicating active bedform migration (Table 2). The unit mostly infills the underlying topography where it overlies H1 or H2. In places where unit BB3 overlies the margins of unit BB2, an erosional lower surface is present (H3, between BB2 and BB3) as a high-amplitude reflection (e.g. Fig. 3a at 10–12 km). On the gridded thickness maps (Fig. 4), unit BB3 is seen to be laterally sandwiched between the multiple infill structures of unit BB2 in the northern part.

of the study area. Unit BB3 is generally thinner than 2.5m but can reach a thickness of up to 9m. Unit BB3 is mostly overlain by unit BB4b with the boundary (H4b) between the units visible as a high-amplitude reflection, varying from conformable to erosional (Fig. 3). The acoustically transparent character of unit BB3, interpreted to reflect sandy sediments, together with the presence of bedforms, indicates that the unit represents a phase of higher-energy conditions than during deposition of unit BB2.

Unit BB4 is subdivided into two sub-units. The lower subunit BB4a appears to be a local feature occurring as an elongated and curved sedimentary package in the central and southern parts of the study area. It extends over 20 km in length and up to 10 km in width (Fig. 4). Where the unit is thickest (up to 20 m), it fills a deep erosional feature (Fig. 3b from 7 to 12 km) down to a depth of ca. –59 m LAT. The lower bounding surface of subunit BB4a largely corresponds to the base of the Brown Bank Fm (H1). As such, this erosional feature is also visible on the gridded depth map of the base of the Brown Bank Fm (Fig. 2a). Only in the most eastern part of the study area, subunit BB4a overlies unit BB3, with an erosional contact between the two units (H4a; Fig. 3b at 11–13 km), which indicates that deposition of unit BB4a occurred after unit BB3. Subunit BB4a can be further subdivided into several (up to ten) stacked sedimentary packages bounded by minor erosional surfaces and all characterised by west-south-westward dipping continuous, medium- to high-amplitude reflections, downlapping onto H1 or an internal erosional surface (Fig. 3b, 8–12 km). This stacked complex indicates a dynamic environment at the time of deposition with sediments prograding westward and infilling a large, elongate depression. The top of

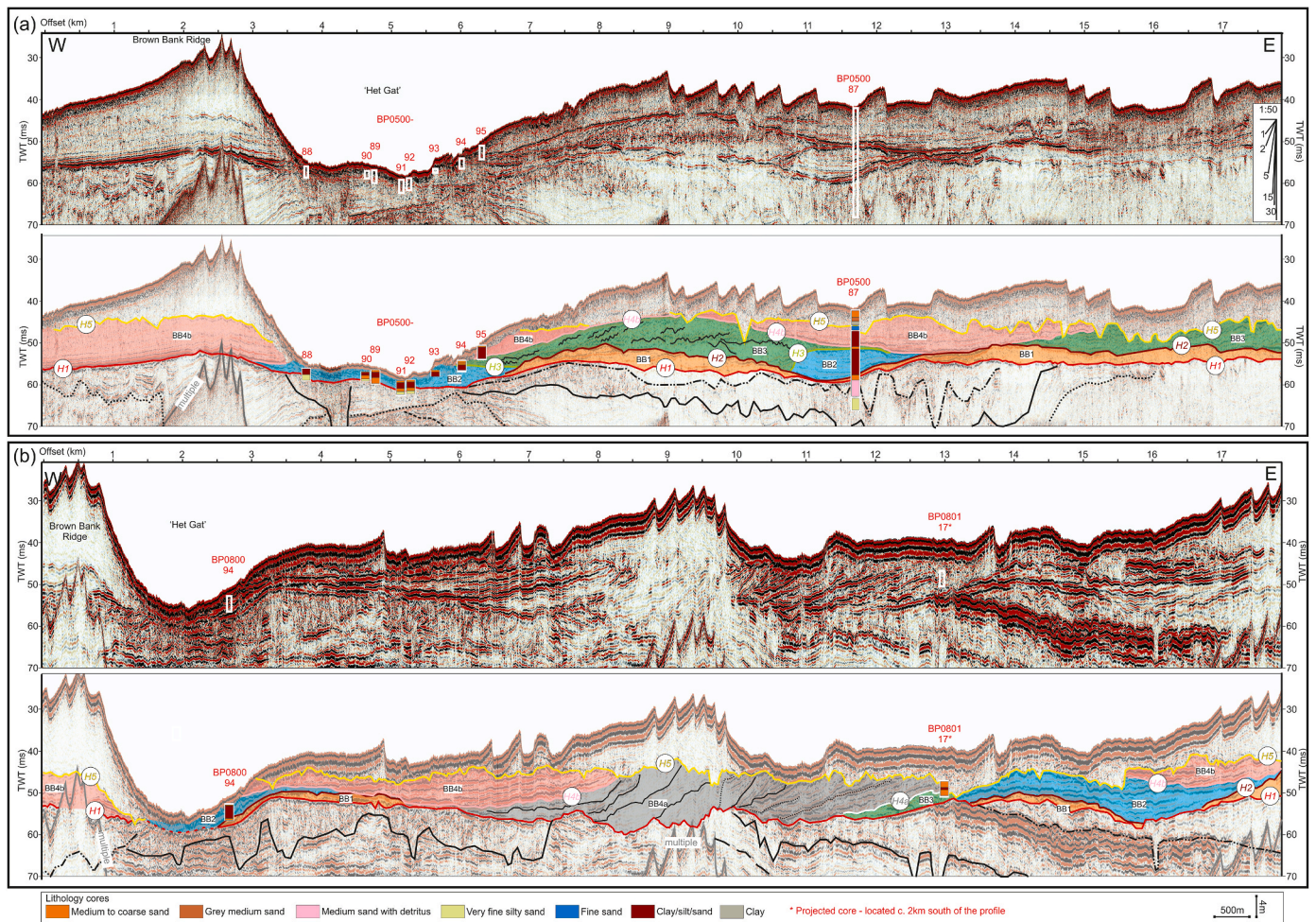


Fig. 3. Two W-E-oriented seismic reflection lines (Sparker data) and the location of some of the cores. The location of the lines is shown in Fig. 1. Profile (a) was acquired in 2023 (Centipede source, SIG dual-channel streamer) and profile (b) was acquired in 2021 (GSO360 source, SIG multi-channel streamer).

the unit is truncated almost everywhere by the high-amplitude and erosional horizon H5, and appears to be overlain by sediments that post-date the Brown Bank Fm (Fig. 3b at 8–13 km). Only on the most westward side, subunit BB4a seems to be unconformably overlain by subunit BB4b (Fig. 3b 6–8 km).

Subunit BB4b can overlie any of the previous units and represents the top seismic unit of the Brown Bank Fm, which does not occur above ca. –30 m LAT in the study area. The unit consists of continuous, high-amplitude reflections, becoming more chaotic towards the top (Table 2). To the east of the Brown Bank Ridge (Fig. 4), it infills the underlying topography - which forms wide troughs - but simultaneously displaying low-angled progradation in a westward direction (Fig. 3a from 6 to 15 km and Fig. 3b from 3 to 18 km). The subunit is generally thinner than 5 m, but locally reaches up to 7.5 m in the eastern section. To the west of the Brown Bank Ridge (Figs. 3a, 0–3 km and Fig. 3b 0–1 km), the unit becomes less confined by the pre-existing topography and features a thick sediment package up to ca. 10 m thick, with a clear westward progradation of downlapping reflections. Whilst the seismic facies is similar to that of unit BB2, the frequency of the internal reflections is higher. The seismic facies is interpreted as indicative of laminated sediments. The thickness maps (Fig. 4) show evidently wider infill structures of BB4b to the east of the Brown Bank Ridge (up to 5 km). These are oriented NNE-SSW, in contrast to the narrower, sinuous N-S-oriented infill structures of unit BB2. The sediments of unit BB4b most likely were sourced from the ENE of the study area under relatively calm conditions. The top of BB4b is truncated by the erosional surface H5, characterised by a continuous medium-to high-amplitude reflection

occurring between ca. –30 and –46 m LAT, and displaying distinct ridges and troughs (Fig. 2c).

4.2. Lithofacies

The main lithofacies distinguished in the cores are summarised in Table 3. The boundaries of the lithofacies have been matched to the seismic interpretations to link them to the seismic units and subunits. The lithofacies are labelled in stratigraphic order, starting with lithofacies observed in unit BB1.

Lithofacies LF1, 2, 3 and 7 are mainly sand lithofacies, and the distinction between them is based on grain size and shape, sorting, presence/absence of laminae, and pebble and shell content. Lithofacies LF4, 5 and 6 mainly consist of clays with different degrees of bioturbation and lamination. All lithofacies except for LF6 are present in a single seismic unit, while LF6 occurs in seismic units BB2 and BB4b (Table 3). In addition, more than one lithofacies may be present within a seismic unit. For example, unit BB2 either consists of a fining upwards succession of LF2, LF3 and LF4, or it contains lithofacies LF5 or LF6.

Lithofacies LF1 consists of medium to coarse sand, which was generally dark coloured or black when opened, and turned orange after oxidation. The sediments contain occasional pebbles and shells. In some locations the top contains iron or carbonate concretions. As LF1 is only present in unit BB1, it shows that seismic unit BB1 was likely deposited by migrating sand waves in a high-energy continental-shelf setting, similar to the one dominating the North Sea offshore the Netherlands today. Lithofacies LF2 consists of a matrix-supported bio- and

Table 2

Characteristics of the different seismic units within the study area, the nature of the bounding surfaces and an interpretation based on the seismic data.

Seismic facies sequences and bounding surfaces	Reflection geometry / configuration	Reflection continuity amplitude, frequency	Reflection terminations (at boundaries)	Example	Interpretation
	East of BB Ridge	Gentle tangential oblique fill or progradation, often becoming chaotic towards the top	Continuous; high amplitude; high frequency; often chaotic towards top	Infilling underlying topography, mostly downlapping westward; erosional truncation at top	Westward progradation of laminated sediments, infilling irregular underlying topography
	West of BB Ridge	Low-angled progradation, often becoming chaotic towards the top; sheet-like	Continuous; high amplitude; high frequency; often chaotic towards top	Downlapping westward; erosional truncation at top	Westward progradation of laminated sediments
		Complex fill, westward prograding parallel or tangential	Continuous; medium to high amplitude; high frequency	Downlap; erosional truncation at top	Prograding sediment lobe, regressive deposit
		Lens shaped, mostly reflection-free at base, becoming more chaotic towards top (with migrating wave structures)	Discontinuous; low amplitude at base, becoming higher amplitude towards top; chaotic	Infilling underlying topography; apparent or erosional truncation at the top	Sand body, mobile/migrating bedforms at the top
		Divergent fill, some onlap on sides	Continuous; medium amplitude; medium frequency	Mostly draping underlying topography, with some onlap; truncated at the top	Gully, channel or topographic low filled with laminated sediment
		Mostly reflection free, some wavy reflections towards top	Mostly transparent	Overlying erosional lower boundary; wavy upper boundary	Sand waves, shaped by shallow-marine processes

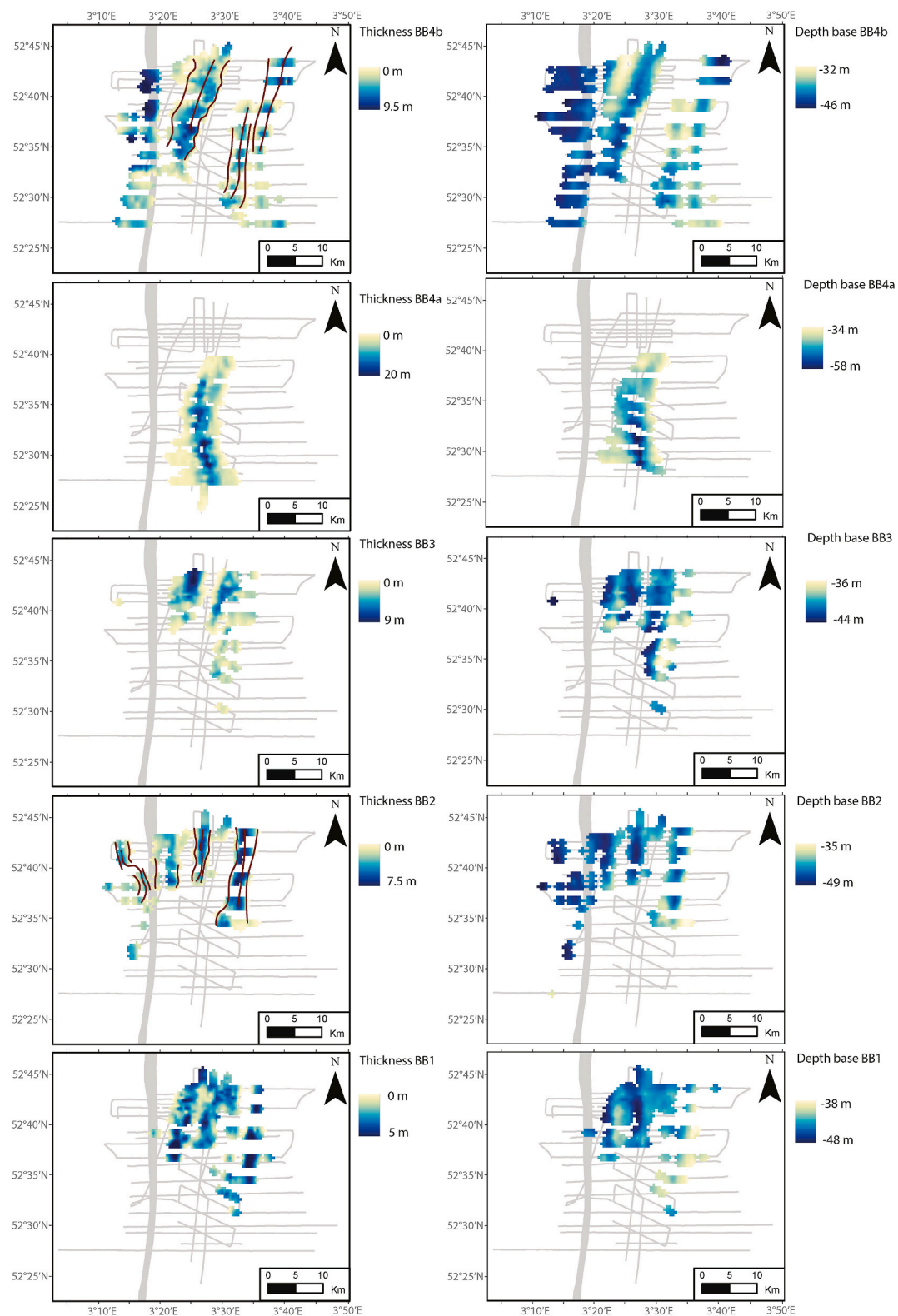


Fig. 4. Distribution and thickness of all seismostratigraphic units of the Brown Bank Fm. Units BB2, BB4a and BB4b are mainly constrained to underlying trough structures, and the outlines and deepest parts of these troughs are indicated by dark lines. The location of the Brown Bank Ridge is indicated in grey for reference. (For interpretation of the references to colour in this figure legend, the reader is referred to the Web version of this article.)

siliciclastic gravel. It is a thin interval (less than 10 cm) and is only found at the base of unit BB2. LF2 may be interpreted as the base of a scour hole or channel. Lithofacies LF3 consists of a fining upwards dark grey sand to silt with occasional clear banding. LF3 may be interpreted as the

infill of an abandoned scour hole or channel under decreasing energy. Lithofacies LF4 consists of a structureless dark grey stiff clay. It has some mottling, mostly at the top. LF4 may be interpreted as the final infill of an abandoned scour hole or channel under low energy conditions.

Lithofacies LF5 consists of a strongly mottled grey silty clay with fine sand and silt patches. LF5 may be interpreted as a relatively low-energy depositional environment, with relatively low sedimentation rates or oxic bottom conditions. Lithofacies LF6 consists of a grey clay with mm- to cm-thick laminae consisting of silt to fine sand, and contains some sandy-clay intervals and some small mottling. LF6 may be interpreted as a relatively low-energy depositional environment, with relatively high sedimentation rates or dysoxic bottom conditions. Lithofacies LF2, 3, 4, 5 and 6 may all be present within unit BB2 which are all indicative of decreasing- or low-energy depositional conditions. Lithofacies LF7 consists of poorly sorted, medium to coarse shell rich sands with thin mud layers. LF7 is present only in unit BB3 and may be interpreted as a mid-to high energy shelf setting with migrating sand waves. Unit BB4b, consisting of LF6, indeed contains laminated sediments, as expected from the seismic facies.

4.3. Luminescence dating

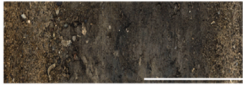
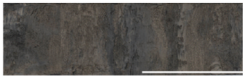

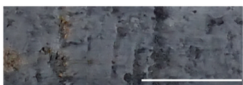
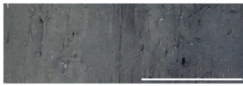
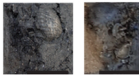
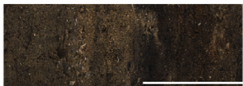
The newly obtained luminescence dating results are combined with previously reported dates from the Brown Bank Fm. Quartz OSL ages reported here for samples from project NCL-3120 (cores BP080094 and BP080095) are slightly older than the ages reported in [Waajen et al. \(2024a\)](#), while they are based on the same measurements. This difference is the result of slight modifications which were made in the data analysis to avoid inaccuracies in results for samples with natural quartz OSL signals plotting relatively high on the dose response curve. These changes are: 1) We used an exponential plus linear fitting of the growth curves, as this provides a better fit for the data compared to the single saturating exponential used for [Waajen et al. \(2024a\)](#). 2) We adopted less stringent criteria for iterative removal of outliers from the equivalent dose distribution, to avoid bias towards younger equivalent doses for skewed dose distributions. 3) Given that all samples share a similar provenance, we used project-averaged estimates to assess the onset of saturation (D0) which were then used to infer the percentage of single-aliquot De estimates above 2D0. This has no effect on the age obtained but does result in a different assessment of validity for some samples.

Due to the different approaches applied by the two different labs, comparison of the age results between the two facilities should be handled with care. As the results between the facilities are similar, we do include the results from both facilities to study age-variations throughout the different units and calculate the mean age per unit. The palaeodoses and dose rates vary between different units within the Brown Bank Fm ([Table 4](#)). Variations in dose rate follow differences in the lithology through the deposits, with the finer-grained deposits characterised by higher dose rates, consistent between the labs. Dose rates for the feldspar fraction are greater than dose rates for the quartz fraction of the same sample due to a contribution from internal K-40. Variations in palaeodoses reflect both variations in depositional age and dose rate. There is little evidence for poor bleaching of the quartz OSL signals; ages obtained using the (slower bleaching) feldspar pIRIR signal are similar to, or even younger than, those obtained using quartz OSL. For some samples, quartz OSL ages could not be determined accurately as the OSL signals were too close to saturation. For those samples, we present minimum ages (CERSA-samples) and questionable ages (NCL-samples), where the difference is the result of differing protocols between labs (see [Waajen et al., 2024a](#) and [appendix A](#)). The results presented in [Table 4](#) are grouped per seismic unit, and include the adjusted luminescence ages from [Waajen et al. \(2024a\)](#), which were used to calculate the mean age of the units. Details on the results are provided in [appendix A](#).

Sediments underlying the Brown Bank Fm have been dated in core BP050087 to the Middle Pleistocene ([Table 4](#)). The quartz OSL results have high levels of saturation, providing poor (doubtful) age constraints. The feldspar pIRIR results are more reliable in these older sediments, but the ages are not in stratigraphic order. The feldspar pIRIR samples with a

Table 3

Lithofacies described from all 18 sediment cores used in this study. Core photos have the top on the left. The white scale bar represents 10 cm and the black scale bar 5 cm.

Lithofacies	Present in seismic unit(s)	Present in cores	Photo
LF7 shell-rich sands w. mud layers	BB3	BP050094, BP080114, BP050087, BP080117	
LF6 Laminated silty clays	BB2; BB4b	BP050095, BP050095, BP080113, BP080114, BP080115, BP050087, BP080094, BP080095, BP080111	
LF5 Strongly mottled silty clays	BB2	BP050087, BP080111, BP080094, BP080095	
LF4 Dark grey stiff clays	BB2	BP080112, BP050091, BP050092, BP050093, BP050094, BP050088, BP050089, BP050090	
LF3 Fining upwards sands to silts	BB2	BP050088, BP050089, BP050091, BP050092	
LF2 Bio- and siliciclastic gravels	BB2 (base only)	BP050088, BP050089, BP050091, BP050092, BP080113	
LF1 iron-rich sands, occasional shells and concretions	BB1	BP080094, BP080095, BP080111, BP080112, BP080113	

validity of 'likely OK' provide ages between 255 and 400 ka.

Unit BB1 contains massive medium to coarse sand, belonging to facies LF1. Quartz dose rates and palaeodoses are low, and none of the samples approached quartz OSL saturation. Quartz OSL dates from unit BB1 are therefore considered reliable. Feldspar pIRIR was only measured on two samples, providing ages that are ca. 21 % younger than the quartz OSL dates obtained on the same samples. This suggests that anomalous fading or inadequate sensitivity correction affects the feldspar ages, indicating that quartz OSL results are more reliable. The unweighted mean age and standard deviation of unit BB1 is 95.3 ± 7.1 ka ($n=4$) based on quartz OSL, and 71.6 ± 0.8 ka ($n=2$) based on feldspar pIRIR ([Fig. 5](#)), including all samples from different cores with a validity 'likely OK' ([Table 4](#)).

The samples measured for luminescence dating from unit BB2 contain heterogeneous sediments with clay and silty/sandy intervals, belonging to LF5 and LF6. The quartz dose rates and palaeodoses are high, and many samples show signs of saturation (>35 % of equivalent doses $> 2D0$; [Table 4](#)). The samples with fewer accepted aliquots above $2D0$ tend to provide older ages, indicating that the results for samples close to saturation (with a validity of 'minimum age' and 'questionable') underestimate the true depositional age. Feldspar pIRIR ages are similar

Table 4

Luminescence results from different Brown Bank units (color-coded following Fig. 3), including underlying (pre-BB) and overlying (post-BB) deposits, measured on different cores and in two different labs. One C14 date, measured at Groningen centre for isotope research, is included (green text) for context. Two outliers defined in Waajen et al. (2024a) are excluded. For all samples, results based on quartz OSL are shown (black), while for a subset also feldspar pIRIR results are obtained (indicated in blue italic text). For some samples, the results from grain-size fractions of both 150–250 μm^a and 90–150 μm^b are provided. For one sample, the quartz OSL was measured on the 90–212 μm^c fractions and feldspar pIRIR on the 180–250 μm^d fraction. When nothing is indicated, the 212–250 μm grain-size fraction was used. *Modified results of the samples published in Waajen et al. (2024a).

Seismic unit	Labcode	Core	Depth (m bsf)	Palaeodose	Dose rate (Gy/ka)	Mean Age (ka)	Mean age +/- 1 sigma error	Comments	Validity
Post-BB	NCL-3223023	BP050087	1.44	65.8 \pm 2.5 <i>76.1 \pm 6.3</i>	1.24 \pm 0.05 <i>2.18 \pm 0.11</i>	52.9 <i>34.9</i>	49.9 - 55.9 <i>31.5 - 38.3</i>	3% >2D0 <i>0% > 2D0</i>	Likely OK <i>Likely OK</i>
Post-BB	GrM-35722	BP050087	2.51	xxx	xxx	>40	xxx	14C date (BP)	
Post-BB	NCL-3223024	BP050087	3.48	107.5 \pm 8.2 <i>149.3 \pm 10.9</i>	1.85 \pm 0.11 <i>2.94 \pm 0.13</i>	58.1 <i>50.8</i>	52.6 - 63.6 <i>46.5 - 55.1</i>	10% >2D0 <i>14% > 2D0</i>	Likely OK <i>Likely OK</i>
BB4b	NCL-3223025	BP050087	4.49	164.7 \pm 14.7 ^c <i>168.9 \pm 17.4^d</i>	2.42 \pm 0.16 ^c <i>3.32 \pm 0.17^d</i>	68.0 <i>52.5</i>	60.5 - 75.5 <i>46.4 - 58.6</i>	43% >2D0 <i>11% > 2D0</i>	Questionable <i>Likely OK</i>
BB4b	NCL-3223026	BP050087	6.27	135.7 \pm 14.8 <i>197.8 \pm 38</i>	2.26 \pm 0.14 <i>3.20 \pm 0.17</i>	59.9 <i>61.8</i>	52.4 - 67.4 <i>49.5 - 74.1</i>	30% >2D0 <i>25% >2D0</i>	Likely OK <i>Questionable</i>
BB3	NCL- 3223027	BP050087	7.29	71.1 \pm 3.9 <i>103.5 \pm 5.6</i>	0.91 \pm 0.05 <i>1.85 \pm 0.11</i>	78.3 <i>56.0</i>	72.0 - 84.6 <i>51.5 - 60.5</i>	3% >2D0 <i>7% >2D0</i>	Likely OK <i>Likely OK</i>
BB3	CERSA443/15	BP080117	1.15	102.31 \pm 21.52 ^a	1.44 \pm 0.16	73.83	58.94 - 88.72	30% >2D0 Poorly bleached	Minimum age
BB3	CERSA443/16	BP080117	1.20	68.89 \pm 8.00 ^a	0.96 \pm 0.10	71.41	63.12 - 79.7	21.4% >2D0 Poorly bleached	Minimum age
BB3	CERSA443/17	BP080117	1.26	55.86 \pm 9.80 ^a 62.42 \pm 7.86 ^b	0.76 \pm 0.08 ^a 0.74 \pm 0.08 ^b	78.55	67.87 - 89.23	12.5% >2D0	Likely OK
BB3	CERSA443/21	BP080117	1.50	59.43 \pm 4.16 ^b	0.77 \pm 0.08	77.15	71.75 - 82.55	4.2% >2D0	Likely OK
BB3	CERSA443/22	BP080117	1.61	58.60 \pm 4.63 ^b	0.84 \pm 0.10	70.18	64.68 - 75.68	0% >2D0	Likely OK
BB3	CERSA443/23	BP080117	1.70	65.09 \pm 4.49 ^b	0.84 \pm 0.10	73.37	64.29 - 82.45	0% >2D0	Likely OK
BB3	CERSA443/32	BP080117	2.55	71.42 \pm 6.04 ^b	0.88 \pm 0.12	80.82	73.98 - 87.66	4.2% >2D0	Likely OK
BB3	CERSA443/33	BP080117	2.65	70.31 \pm 6.47 ^b	0.89 \pm 0.12	82.85	76.11 - 89.59	8.3% >2D0	Likely OK
BB2	CERSA477/10	BP080111*	0.95	129.8 \pm 7.7 ^a 115.6 \pm 10.1 ^b	2.00 \pm 0.21 ^a 2.06 \pm 0.21 ^b	64.7	61.2 - 68.2	62.5% >2D0	Minimum age
BB2	CERSA477/12	BP080111*	1.05	114.5 \pm 11.2 ^a	1.67 \pm 0.17	68.8	62.1 - 75.5	66.7% >2D0	Minimum age
BB2	CERSA477/31	BP080111*	2.31	87.3 \pm 7.4 ^a 105.9 \pm 12.0 ^b	1.82 \pm 0.18 ^a 1.87 \pm 0.19 ^b	57.9	52.6 - 63.2	62.5% >2D0	Minimum age
BB2	CERSA477/32	BP080111*	2.34	107.4 \pm 11.2 ^a 98.0 \pm 9.5 ^b	1.43 \pm 0.15 ^a 1.47 \pm 0.15 ^b	68.9	63.7 - 74.1	76.3% >2D0	Minimum age
BB2	CERSA477/33	BP080111*	2.37	96.0 \pm 11.3 ^b	1.17 \pm 0.12	81.9	72.2 - 91.6	40% >2D0	Minimum age
BB2	NCL-3120121	BP080094*	0.70	120.1 \pm 7.6 <i>161.7 \pm 5.1</i>	1.48 \pm 0.06 <i>2.26 \pm 0.16</i>	81.2 <i>76.4</i>	75 - 87.4 <i>70.4 - 82.4</i>	27% >2D0 <i>0% >2D0</i>	Likely OK <i>Likely OK</i>
BB2	NCL-3120122	BP080094*	1.55	149.8 \pm 10.4	1.60 \pm 0.07	93.4	85.9 - 100.9	39% >2D0	Questionable
BB2	NCL-3120124	BP080095*	1.50	153.0 \pm 7.4 <i>149.9 \pm 5.0</i>	1.51 \pm 0.06 <i>2.29 \pm 0.16</i>	101.6 <i>69.9</i>	94.8 - 108.1 <i>64.4 - 75.4</i>	53% >2D0 <i>0% >2D0</i>	Questionable <i>Likely OK</i>
BB2	NCL-3223028	BP050087	9.63	133.7 \pm 10.3 <i>197.1 \pm 52.1</i>	1.99 \pm 0.13 <i>3.24 \pm 0.13</i>	67.2 <i>60.8</i>	60.5 - 73.9 <i>44.5 - 77.1</i>	28% >2D0 <i>22% >2D0</i>	Likely OK <i>Likely OK</i>
BB2	NCL-3223029	BP050087	11.22	137.3 \pm 9.8 <i>176.3 \pm 27.4</i>	1.72 \pm 0.11 <i>2.66 \pm 0.14</i>	80.0 <i>66.4</i>	73.4 - 87.6 <i>55.5 - 77.3</i>	24% >2D0 <i>50% >2D0</i>	Likely OK <i>Likely OK</i>
BB2	NCL-3223030	BP050087	12.23	128.0 \pm 9.2 <i>189.6 \pm 12.8</i>	1.73 \pm 0.12 <i>2.67 \pm 0.15</i>	74.2 <i>71.1</i>	66.9 - 81.5 <i>64.8 - 77.4</i>	23% >2D0 <i>33% >2D0</i>	Likely OK <i>Likely OK</i>
BB1	CERSA477/36	BP080111*	2.59	73.8 \pm 3.1	0.82 \pm 0.11	89.6	85.8 - 93.4	16.7% >2D0	Likely OK
BB1	CERSA477/37	BP080111*	2.64	68.8 \pm 4.1	0.78 \pm 0.11	88.7	83.4 - 94	20.8% >2D0	Likely OK
BB1	NCL-3120123	BP080094*	2.85	73.0 \pm 3.5 <i>101.3 \pm 4.2</i>	0.71 \pm 0.04 <i>1.50 \pm 0.15</i>	102.2 <i>72.2</i>	94.8 - 109.6 <i>64.2 - 80.2</i>	2% >2D0 <i>3.4% >2D0</i>	Likely OK <i>Likely OK</i>
BB1	NCL-3223031	BP050087	13.14	64.7 \pm 2.9 <i>112.4 \pm 5.8</i>	0.64 \pm 0.03 <i>1.58 \pm 0.10</i>	100.6 <i>71.0</i>	94.6 - 106.6 <i>65.2 - 76.8</i>	0% >2D0 <i>23% >2D0</i>	Likely OK <i>Likely OK</i>
Pre-BB	NCL-3223032	BP050087	15.01	244.5 \pm 15.8 <i>825.5 \pm 69.8</i>	1.10 \pm 0.04 <i>2.04 \pm 0.10</i>	221.4 <i>404.0</i>	204.7 - 238.1 <i>364.1 - 443.9</i>	84% >2D0 <i>92% >2D0</i>	Doubtful <i>Questionable</i>
Pre-BB	NCL-3223033	BP050087	18.00	303.1 \pm 20.6 <i>795.3 \pm 15.9</i>	2.03 \pm 0.09 <i>2.97 \pm 0.13</i>	149.6 <i>268.2</i>	137.4 - 161.8 <i>255.1 - 281.3</i>	86% >2D0 <i>93% >2D0</i>	Doubtful <i>Likely OK</i>
Pre-BB	NCL-3223034	BP050087	19.85	295.6 \pm 19.9 <i>823.4 \pm 46.1</i>	1.27 \pm 0.05 <i>2.21 \pm 0.11</i>	232.3 <i>372.3</i>	214.6 - 250.0 <i>344.8 - 399.8</i>	91% >2D0 <i>98% >2D0</i>	Doubtful <i>Likely OK</i>

to the quartz OSL ages, indicating that either fading does not influence feldspar age results, or that both the quartz OSL and feldspar pIRIR results underestimate the true age. The unweighted mean age and standard deviation of unit BB2 is 75.7 ± 6.4 ka ($n=4$) based on quartz OSL, and 68.9 ± 5.8 ka ($n=5$) based on feldspar pIRIR (Fig. 5), including samples from different cores with a validity 'likely OK' (Table 4).

Unit BB3 contains sand-rich deposits, in some intervals with silty clay laminae. Samples from unit BB3 have lower quartz dose rates compared to the clay intervals of units BB2 and BB4b. The quartz equivalent dose results do not show signs of saturation (all samples <35 % above 2D0). The unweighted mean age and standard deviation of unit BB3 is 77.3 ± 4.3 ka ($n=7$) based on quartz OSL (Fig. 5), including samples from different cores with a validity 'likely OK' (Table 4). Feldspar pIRIR is only measured in 1 sample, and the resulting age is 27 % younger compared to mean quartz.

Unit BB4a has not been cored and therefore not been dated. Unit BB4b contains laminated clays, with limited sand content. The samples have a high dose rate. Sample NCL-3223025 does not contain quartz grains of the 212–250 μm grain-size fraction, consequently quartz OSL was measured on smaller grain size compared to the other samples. The samples have relatively high percentages above 2D0, indicating saturation might influence the results. Feldspar pIRIR results are similar to the quartz ages. There is only one reliable quartz OSL and one reliable feldspar pIRIR result (Table 4).

Sediments above the Brown Bank Fm have also been dated in core

BP050087. The laminated fine sand, present above BB4b at 3–4 m depth, has an age between 46 and 64 ka (including both reliable quartz OSL and feldspar pIRIR results). Above this sand is an additional clay-rich interval (2.1–3 m), from which organic-rich sediment samples were sieved and the organic plant residue was used for radiocarbon dating at the Centre for Isotope Research at the University of Groningen. Both samples, GrM-35720 and GrM-35722 yielded ages $>40,000$ ^{14}C yr BP. The medium sands above this clay-rich interval show no signs of saturation, and had feldspar pIRIR result of 31–38 ka, and a quartz OSL result of 50–56 ka.

In general, the OSL ages show a normal sequence with younger ages in stratigraphically higher units (Fig. 5). The quartz OSL age of unit BB2 is nearly identical to that of overlying unit BB3, indicating they are of similar age. Unit BB1 is clearly older, and unit BB4b is clearly younger.

4.3.1. Reasons for age underestimation

There are multiple lines of evidence which suggest that luminescence ages from the laminated clay-rich marine deposits may underestimate the true age. Here we outline this evidence, and also pose a hypothesis of the causes.

The first line of evidence is based on a comparison of the quartz OSL and feldspar pIRIR results. We note that for the sandy units, the feldspar ages tend to be approximately 25 % younger than the quartz OSL ages, and we attribute this difference to anomalous fading, inadequate sensitivity change correction in feldspar and/or inadequate assumptions

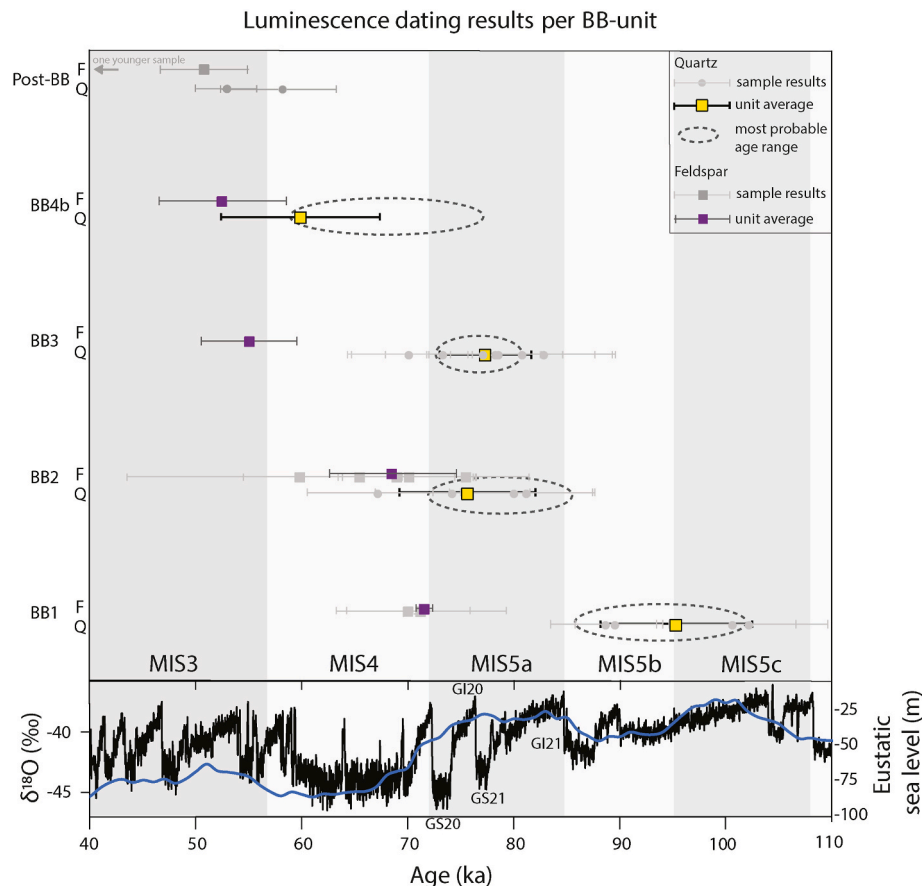


Fig. 5. Luminescence age results per seismostratigraphic unit of the Brown Bank Fm. Quartz OSL results are visualised at the base (Q), feldspar pIRIR results above (F). Individual results (in grey) include only those with a validity of 'likely OK' and the unweighted means with standard deviation are coloured (yellow quartz OSL, purple feldspar pIRIR results). The dashed ellipses indicate the most probable age ranges as discussed in 4.3.1. The eustatic sea level curve (Spratt and Lisiecki, 2016) and NGRIP $\delta^{18}\text{O}_{\text{ice}}$ record (North Greenland Ice Core Project (NGRIP) Members, 2004; Wolff et al., 2010) are provided on the same time scale, and the Greenland Stadials (GS) and Greenland Interstadials (GI) are annotated. (For interpretation of the references to colour in this figure legend, the reader is referred to the Web version of this article.)

on internal potassium content from the measured grains. Such problems are expected to occur for all samples, but the quartz and feldspar results are within error range for the clay rich units BB2 and BB4b. This implies that either the problems with feldspar are context dependent, and do not occur in these clay-rich units, or that both feldspar pIRIR and quartz OSL results underestimate the depositional age within the clay-rich units.

The first possible cause for quartz OSL age underestimation is the saturation of the OSL signal. For units BB2 and BB4b, many of the palaeodose estimates were indeed unreliable due to saturation. Results of the more ‘reliable’ quartz OSL samples from these units are however not always higher than the ‘questionable’ and ‘minimum’ age samples.

Another hypothesis to explain the trends observed is that the age underestimation and the alignment of quartz OSL and feldspar pIRIR ages are caused by dose rate heterogeneity in laminated sediments. In laminated clays, the sand grains on which the palaeodose is measured, are dominantly present in sand laminae and may experience lower dose rates than calculated based on the bulk material. It is well known that the dose rate varies with the lithology of the material (Narayana and Rajashekara, 2010). Radionuclide concentrations tend to be (much) higher in fine-grained material, resulting in greater dose rates. Gamma rays penetrate ca. 20–30 cm in sediments, resulting in a uniform gamma dose rate throughout the laminae. However, beta particles only travel a few mm, and as a consequence, the external beta dose rate will be lower in the sandy laminae than in the clayey bulk sediment. Although the dose rate of both quartz and feldspar grains is affected, the relative effect on feldspar will be smaller as the dose rate also contains a contribution from internal K in the K-rich feldspars used for measurement.

Thus, dose rate heterogeneity in laminated sediments would result in an overestimation of the dose rate for sand grains in sandy laminae and would affect quartz ages more severely than feldspar ages. Younger ages than expected in (laminated) clay-rich sediments have also been described onshore the Netherlands (Busschers et al., 2007), indicating this may be a wider issue and not only present within the sediments of the Brown Bank Formation.

Within core BP050087, which captures all BB units that were dated, the OSL ages are generally in sequence. The age results from the sediment directly above unit BB4b (3.48 m depth) are not much younger than the results from unit BB4b, but older than 40 ka as indicated by ^{14}C date at 2.51 m, constraining the maximum error margin of the OSL ages of unit BB4b on their lower end. Based on the current understanding of luminescence dating, we assume the provided quartz OSL ages are correct for sandy units BB1 and BB3 and provide minimum ages for the clayey units BB2 and BB4b. This is visualised by the dashed ellipses in Fig. 5, where the minimum ages for units BB2 and BB4b are based on the standard deviation of the mean quartz OSL age in combination with the age difference between the quartz and feldspar results in units BB1 and BB3. Due to these minimum ages, unit BB4 is more consistent with an age which can be correlated to the MIS 5a-4 transition than to MIS 3, which will be further discussed in section 4.5.

4.4. Palaeoenvironmental proxies

Proxy results from pollen, diatoms, molluscs and geochemical analyses all provide further constraints on the depositional environments and local setting of the Brown Bank units. The pollen results of BP050087, showing changes in regional vegetation through time, are presented in Fig. 6. Diagrams on salinity and lifeform characteristics based on diatom data are shown in Fig. 7. A percentage diagram of the diatom taxa is provided in the Supplementary Fig. S2. Mollusc abundances, indicators of climate, depositional environment and degree of post-depositional reworking, were too low to present count data and therefore assemblages are qualitatively characterised (Fig. 8). A summary of all proxy data obtained from BP050087, including the lithofacies, seismic units, and the HCA results, is included in Fig. 8.

4.4.1. Units below the Brown Bank formation

Pollen: Pollen zone (PZ)-A is present from the base of the core (20.25 m) to 17.50 m (Fig. 6). This interval has, on average, 72 % Arboreal Pollen (AP), dominated by *Pinus*, *Betula* and *Alnus*. Ericaceae is relatively abundant, as are Poaceae and *Sphagnum*. The pollen assemblage is similar to the Brown Bank Fm (Waajen et al., 2024a), with the main differences being the lower amounts of Cyperaceae and the absence of marine non-pollen palynomorphs (NPP; dinoflagellate cysts and foraminifera). Above PZ-A, there is a sand-rich interval barren in pollen.

Diatoms: Diatoms are rare in these deposits. The samples which contained diatoms are characterized by low total counts. *Delphineis minutissima*, *Cymatosira belgica*, *Staurosirella guenter-grassii* and *Coscinodiscophyceae* have high relative abundances (Fig. S2). In this interval, epiphytes and freshwater to brackish taxa have relatively high abundances (Fig. 7).

Molluscs: These sediments are barren in molluscs.

HCA: The hierarchical cluster analysis (HCA) divides the XRF data of core BP050087 into clusters with geochemical similar compositions and is plotted along the depth of the core in Fig. 8. The elemental data on which the clustering is based, is presented in Fig. S3. The HCA results show that the pre-BB depositional record has a constant geochemical signature, with most sediments assigned to cluster 1, and only the interval 17.50–18.92 m assigned to clusters 4 and 5. This interval contains brown silty sand, and thus has a different sedimentological and geochemical content compared to the grey sands below and above. The long intervals belonging to a single cluster are interpreted as a stable sediment source for most of the pre-BB interval.

4.4.2. Unit BB1 (12.71–13.64 m bsf)

Unit BB1 corresponds with the unit ‘SD’ as described in Waajen et al., 2024a, 2024b. Therefore, the climatological and geochemical interpretations from cores BP08094 and BP080095 (VC35 and VC36 in Waajen et al., 2024a, 2024b) are included for the palaeoenvironmental interpretations.

Pollen: The sediments of unit BB1 are barren in pollen in BP050087 (Fig. 6). In BP08094, low amounts of pollen are present representing Early Glacial interstadial pollen assemblages (presented in Waajen et al., 2024a).

Diatoms: Two samples from unit BB1 were analysed for diatoms, both with very low diatom counts (Fig. 7). Neither fragments nor partially dissolved diatoms or sponge spicules were observed, pointing towards low concentrations instead of poor preservation. The taxa that were present mainly indicate marine and brackish conditions.

Molluscs: The mollusc assemblage in unit BB1 contains a mixture of worn specimens and finely preserved, autochthonous shells with periostracum. The autochthonous assemblage is dominated by *Spisula elliptica* and *Macoma calcarea*, combined with *Astarte montagui* and *Altenium dawsoni*, indicating high-boreal-subarctic marine conditions around or below storm wave base (lower shoreface to inner shelf).

HCA: The geochemical composition of unit BB1 contains intervals of all five clusters, indicating heterogeneous sediments (elemental composition, see Fig. S3). The most representative clusters are clusters 1 and 3, where cluster 1 is dominant in the sediments underlying unit BB1, and cluster 3 mostly present in the sediments overlying unit BB1.

4.4.3. Unit BB2 (7.54–12.71 m bsf)

This unit includes the ‘BB clay unit’ as discussed in Waajen et al., 2024a, 2024b. Therefore, the climatological and geochemical interpretations from cores BP08094 and BP08095 (VC35 and VC36 in Waajen et al., 2024a, 2024b) are included for the palaeoenvironmental interpretations.

Pollen: Two pollen zones (PZ-B and PZ-C) are distinguished in unit BB2. PZ-B is present in the lower half of the unit, ranging from 12.75 to 9.70 m bsf. PZ-B contains, on average, 87 % arboreal pollen (AP) dominated by *Pinus* (around 60 %), but with abundant *Betula* (around

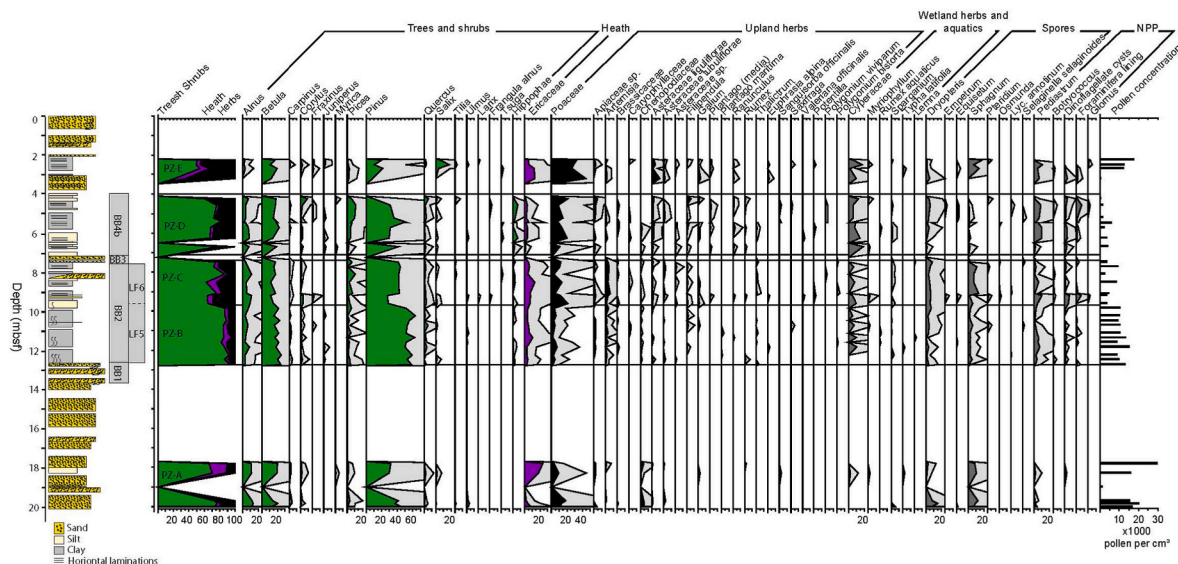


Fig. 6. Pollen diagram of BP050087, including all taxa that are present > 2 % and in at least 2 samples. For clarity, all abundances are exaggerated five times, shown in light grey. Tree and shrub pollen are green, heath is purple, upland herbs black. The pollen, spores and non-pollen palynomorphs (NPP) not included in the pollen sum are dark grey. The diagram is divided in 5 pollen zones (PZ-A to PZ-E). (For interpretation of the references to colour in this figure legend, the reader is referred to the Web version of this article.)

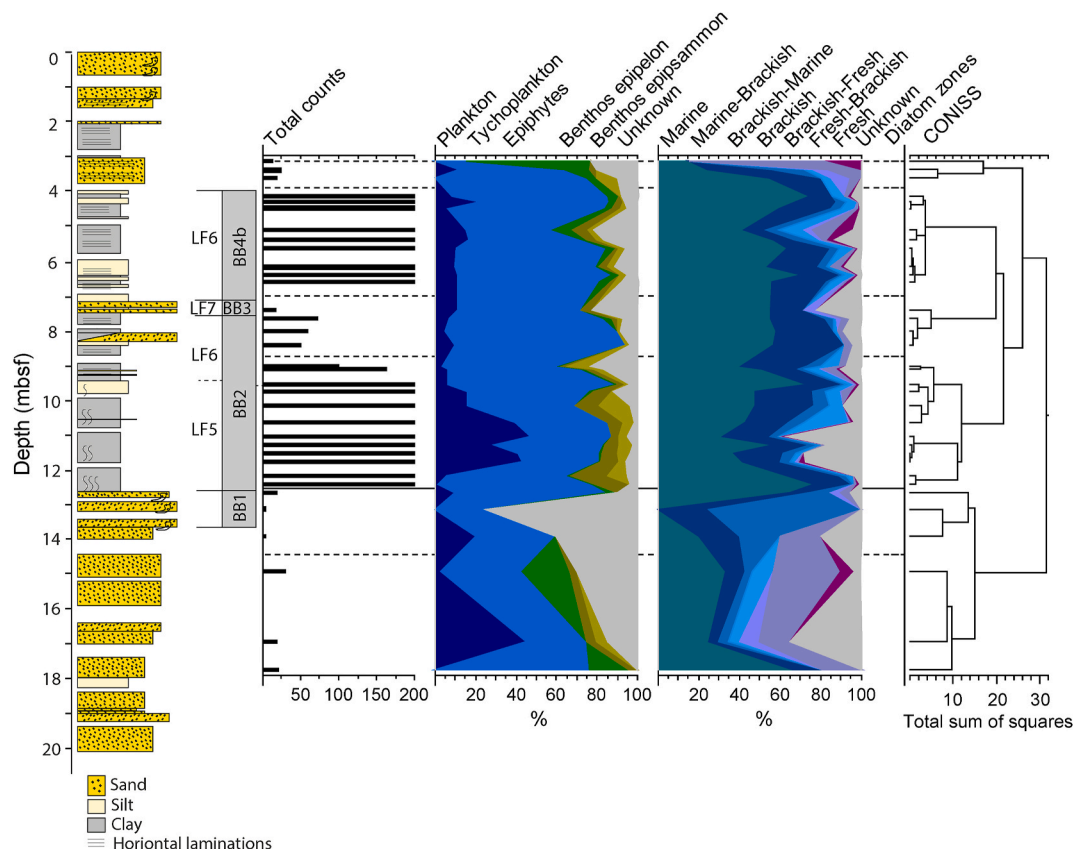


Fig. 7. Diatom data of core BP050087. From left to right: lithological representation of core BP050087, with the depth intervals of the different units indicated; total diatom counts per sample; percentages of the lifeform of the diatom species; percentages of the salinity preference of the diatom species; CONISS zonation of the diatom assemblages. Adapted from Cvetkoska and Verweij (2024).

BP050087

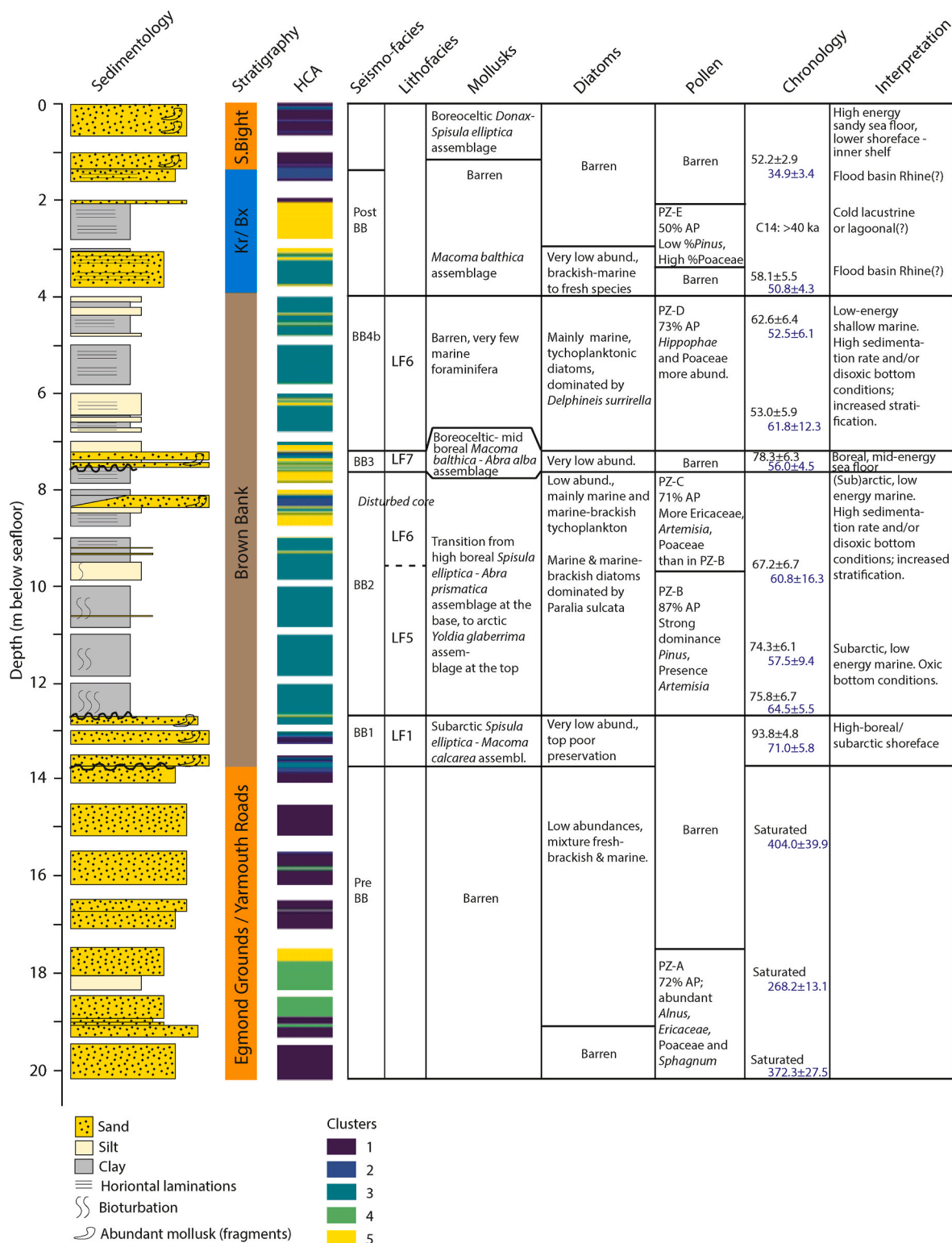


Fig. 8. Compilation of results of core BP050087, containing, from left to right: a sedimentary log, stratigraphic interpretation, results of the Hierarchical cluster analysis (HCA) based on XRF data, seismic units, the lithological facies for the Brown Bank Fm, biofacies of mollusc, diatoms, and pollen assemblages, where the differences in assemblages between zones are highlighted, OSL ages where the upper represent quartz OSL and the lower feldspar PIRIR ages, and the interpretation of the depositional environment. (For interpretation of the references to colour in this figure legend, the reader is referred to the Web version of this article.)

20 %). Thermophilous trees *Corylus* and *Quercus* are present in low amounts, as is *Artemisia*, while Ericaceae, Poaceae and Cyperaceae are more abundant. The transition between PZ-B and PZ-C is abrupt and coincides with the transition from lithofacies LF5 to LF6. However, this lithological transition corresponds to a gradual decrease in the degree of bioturbation, and is not as abrupt as the observed change in the pollen content. PZ-C represents the top half of unit BB2, from 9.70 to 7.45 m bsf and contains, on average, 71 % AP. Although the taxa assemblage is similar to that of PZ-B, PZ-C contains significantly less *Pinus* (ca. 40 %) and *Betula* (ca. 15 %) and more *Alnus*, *Picea*, Poaceae, Ericaceae, *Artemisia* and spores. The pollen concentration is lower in PZ-C than in PZ-B (Fig. 6).

Diatoms: Unit BB2 is characterised by much higher amounts of marine diatoms compared to underlying units (Fig. 7). The zonation of diatom data based on CONISS clearly subdivides unit BB2 into two zones, separated by a boundary that is slightly higher in the core compared to the boundary between pollen zones PZ-B and PZ-C. Between 12 and 10 m bsf (lithofacies LF5), there is a high abundance of planktonic taxa, indicative of relatively deep and open water conditions. Diatom abundances are high in LF5 but decrease within the laminated sediments of lithofacies LF6. As there are no fragments or partially dissolved diatoms, this decrease is interpreted to be caused by lower production rates and not by changes in preservation. In lithofacies LF6 tychoplankton is more abundant, epiphytes occur in low abundances, and planktonic taxa are less abundant compared to lithofacies LF5. In addition, there are more marine-brackish taxa and less fully marine taxa compared to lithofacies LF5. This decrease in diatom counts, marine and planktonic taxa in lithofacies LF6 can be interpreted as shallower water conditions, with a decrease in salinity and potentially colder conditions compared to lithofacies LF5.

Molluscs: The mollusc assemblages in unit BB2 consists of a mixture in preservation, where some molluscs have fine structures preserved with a thick periostracum, indicative of pristine preservation and therefore classified as autochthonous, and others are worn. The autochthonous molluscs all indicate low-energy marine conditions. The assemblages show a transition from lower shoreface-inner shelf high boreal assemblages at the base, dominated by *Spisula elliptica* and *Abra prismatica*, to subarctic assemblages dominated by *Macoma calcarea* in the middle, to arctic assemblages at the top characterised by the dominance of *Yoldia hyperborea* and *Ennucula tenuis*. The foraminifera taxon *Ammonia* is abundant in most samples of unit BB2, especially in the lower and middle part; *Quinqueloculina* only occurs in the top few samples.

HCA: The geochemical signature of unit BB2 mainly corresponds to cluster 3, indicating a different geochemical composition compared to the underlying units. The laminated interval of lithofacies LF6 mainly corresponds to cluster 5 but contains more alternations in geochemical signature.

4.4.4. Unit BB3 (7.20–7.54 m bsf)

Pollen: Unit BB3 in core BP050087 is barren in pollen.

Diatoms: Only one sample from unit BB3 was analysed for diatoms. This sample contained very low diatom abundance, while sponge spicula were abundant. The diatom assemblage is mainly represented by marine and marine-brackish tychoplanktonic taxa and is similar to the underlying and overlying units (Fig. 7).

Molluscs: The mollusc assemblage from unit BB3 has mixed preservation characteristics, where the well-preserved, autochthonous molluscs consist of boreoceltic to mid-boreal low-mid energy sea floor assemblages dominated by *Macoma balthica* and *Abra alba*. As unit BB3 is thin in core BP050087, sediments from unit BB3 from core BP050094 (lithofacies LF7) have also been analysed. These molluscs also have mixed preservation characteristics. The autochthonous molluscs from these sediments represent a transition from sub-arctic sea floor fauna, with the occurrence of *Alteneum dawsoni*, *Astarte montagui* and *Macoma calcarea*, to boreal sea floor fauna at the top, dominated by *Spisula*

elliptica and *Macoma balthica*.

HCA: Unit BB3 samples are mainly assigned to geochemical cluster 5, with some intervals of clusters 3 and 2. While both units BB1 and BB3 are sand-dominated, their geochemical signature is different.

4.4.5. Unit BB4b (4–7.20 m bsf)

Pollen: Pollen zone PZ-D corresponds to the sediment of subunit BB4b, ranging from 7.1 to 4.0 m bsf, and contains, on average, 73 % AP. Dominant taxa are *Pinus*, *Betula* and Poaceae, followed by *Alnus*, *Picea* and Cyperaceae. *Hippophae* is present in the entire interval, which is a major distinction from the other pollen zones. The pollen concentration decreases towards the top of PZ-D. Compared to underlying PZ-C, PZ-D has lower abundances of *Pinus*, Ericaceae and *Sphagnum*. *Artemisia* almost disappears, while there are higher abundances of Poaceae and Cyperaceae.

Diatoms: Diatom counts are high within subunit BB4b (Fig. 7). Although marine and marine-brackish taxa dominate, the amount of brackish and freshwater taxa slightly increases towards the top of unit BB4b. The presence of epiphytes in this interval indicates the proximity to a freshwater source with vegetation. Although units BB2 and BB4b are similar (Fig. 7), the main difference is in the amount of planktonic and tychoplanktonic taxa. In addition, some taxa are present in only one of the two deposits (Fig. S2). Another difference is that the most dominant species in unit BB2 is *Parallia sulcata*, while in subunit BB4b it is *Delphineis surirella*. The combined presence of species such as *Delphineis minutissima*, *Rhaphoneis ampiceros* and *Thalassiosira* sp. point to cold climatic conditions with an open coastal configuration (Denys, 1999; Ribeiro et al., 2021).

Molluscs: Most sediment samples from subunit BB4b were barren in molluscs. Some samples contain small, unidentified mollusc fragments, with mixed preservation characteristics. The autochthonous occurrence of *Spirorbis* in the top sample is indicative of shallow marine conditions and is often related to seagrass debris. Foraminifera *Ammonia* and *Quinqueloculina* are present in most samples, indicating a low energy but well-mixed sea floor.

HCA: The elemental signature of subunit BB4b is very similar to unit BB2, dominated by cluster 3, but with occasional thin intervals of cluster 5 (Fig. 8). This suggests a similar depositional setting and sediment source for both unit BB2 and subunit BB4b.

4.4.6. Overlying Late Pleistocene deposits (1.16–4.00 m bsf)

Pollen: PZ-E is present from 2.1 to 3.2 m bsf, in post-Brown Bank Fm deposits. Samples between 3.2 and 4 m bsf were barren, as were samples above 2.1 m. The first sample containing pollen, at 3.2 m, has a very low pollen concentration (265 grains/cm³), containing 22 % AP and 65 % herbaceous pollen. The samples in the clay interval at 2.1–3 m have high pollen concentrations and contain, on average, 50 % AP, which is dominated by *Pinus*, *Betula*, and *Salix*. *Juniperus*, *Alnus*, *Carpinus*, *Corylus* and *Picea* are present in low amounts. Poaceae, Ericaceae and *Sphagnum* are abundant.

Diatoms: Three diatom samples were analysed in the meter above the Brown Bank Fm (3.00–4.00 m bsf). All samples contained very few diatoms. The samples show a strong increase in epiphytic species, and also contain a high proportion of fresh-brackish and freshwater taxa. This points to a relatively shallow water, fresh(ening) environment with limited marine influence. The sediments above 3.00 m bsf were barren in diatoms.

Molluscs: Most sediments are (almost) barren in molluscs. There is one interval at 3.21–3.29 m bsf which contains well-preserved *Macoma balthica*, *M. calcarea* and *Spisula elliptica*; species representing a low-energy high-boreal-subarctic sea floor. In a few other samples, well-preserved *Spatangus*, *Donax vittatus* and a barnacle are present, indicating of temperate marine sandy sea floor conditions.

HCA: The sand in the meter above the Brown Bank Fm has a similar geochemical signature as units BB4b and BB2, corresponding mainly to cluster 3. The clay above (2–3 m) belongs to cluster 5, and thus has a

different geochemical signature compared to the clays from the Brown Bank Fm, indicating a different depositional environment or sediment source. The top 2 m mainly consist of clusters 1 and 2 and are different from all units in the Brown Bank Fm.

4.5. Depositional environment and temporal evolution of the Brown Bank formation

Combining all proxy results allows an interpretation of the environmental conditions during deposition of the Brown Bank Fm. By combining these with the OSL ages, a correlation can now be established between the different units of the Brown Bank Fm and global climate trends as recorded in the NGRIP record (i.e. Greenland Stadials and Interstadials) (Fig. 5).

4.5.1. Unit BB1 – correlated to early MIS 5a – GI21

Underlying unit BB1 is a regional-scale erosional surface that eroded the underlying Middle Pleistocene sediments. A N-S oriented sandy ridge-swale seabed developed on top of this erosional surface (unit BB1). This seabed formed in a high-boreal-subarctic shallow shelf sea dominated by tidal currents. Locally in swales, non-deposition or further erosion occurred into underlying much older sediments of the Egmond Grounds and Yarmouth Roads Formations. These Middle Pleistocene sediments within core BP050087 were deposited under climatic conditions relatively similar to deposition of the Brown Bank Fm; pollen assemblages neither point to full interglacial nor full glacial conditions.

Mollusc assemblages of unit BB1 indicate that sediments were deposited at or below storm wave base, suggesting water depths of at least 10–15m. In the swales, deposition of sand was limited and/or only lag formation occurred, while the ridges show a thicker sand unit that locally shows exceptionally preserved submarine dune bedform morphology. The N-S orientation of the ridge and swale topography as well as a northward migration of the sand dune bedforms, show resemblance to the sea floor morphology of the present day southern North Sea (Fig. 1).

The pollen record from unit BB1, analysed in core BP080094, suggests that in this phase, terrestrial vegetation consisted of a combination of cool-temperate forests (including *Pinus*, *Alnus*, *Carpinus*, *Corylus* and *Betula*) and grasslands (Poaceae and Cyperaceae), which is in line with reconstructed air temperatures ca. 2.5 °C below present (Waajen et al., 2024b). Although unit BB1 is dated to 88–102 ka, the exceptional preservation of its sand dune bed morphology and concordant draping with clays of overlying unit BB2 (dated to 69–82 ka, see below), makes an hiatus between unit BB1 and BB2 unlikely. Therefore, deposition during the younger end of this age range for unit BB1 is most likely. We therefore suggest that the sediments of unit BB1 represent the final phase of open marine conditions that existed up to the sea-level highstand of MIS 5a or Greenland Interstadial GI21 (Fig. 5). In Europe, this period is also known as the Odderade/St. Germain II interstadial.

4.5.2. Unit BB2 – correlated to MIS 5a – GS21

During the transition from unit BB1 to unit BB2 air temperatures decreased almost 2 °C (Waajen et al., 2024b). At the onset of deposition of unit BB2, major environmental changes occurred that turned the study area into a low-energy depositional setting. Clayey sediments of unit BB2 started to fill the topographic lows of the pre-existing N-S elongated ridge-swale complexes (Fig. 9b). In some of the infills, unit BB2 consists of laminated silty clays (lithofacies LF5 and LF6), draping the underlying topography and, in some instances, fully preserving the dune-shaped bedforms of BB1 (Waajen et al., 2024a), the latter indicating that no or limited erosion occurred between deposition of unit BB1 and BB2, suggesting that the time between deposition of the top of unit BB1 and base of unit BB2 was short. In other areas, the fill consists of bioclastic gravel (LF2) followed by fining upwards sands (LF3) and clays (LF4). Our OSL ages of unit BB2 show a mean age range of 69.3–82.1 ka showing deposition during the latest part of MIS 5a and is

correlated to Greenland Stadial GS21 based on the (exceptional) preservation of bedforms of unit BB1 (Fig. 5).

Within unit BB2 additional cooling is observed in the diatom, mollusc and pollen data, with the largest change at the boundary of lithofacies LF5 to LF6, described in core BP050087, characterised by a decrease in bioturbation. The top of the clay unit in BP080094 (VC35 in Waajen et al., 2024a, 2024b) is now also assigned to pollen zone PZ-C, and the reconstructed cooling in air temperature of ca. 2 °C (based on GDGT-data, Waajen et al., 2024b) is in line with the observed changes in pollen, diatom and mollusc assemblages in this study. The presence of *Artemisia* throughout unit BB2 suggests relatively dry conditions in the terrestrial vegetation. The decrease in bioturbation within unit BB2 is interpreted as indicative of water column stratification and lower bottom oxygen content. During deposition of lithofacies LF5 – described in core BP050087 – there would have been enough mixing of the water column to allow oxic bottom water conditions necessary for the observed bioturbation in the sedimentary record. With increasing climate cooling, water column stratification resulted in dysoxic bottom waters with limited bioturbation. Throughout deposition of unit BB2 open-marine conditions prevailed in a low energy setting.

4.5.3. Unit BB3 – correlated to late MIS 5a – GI20

Deposits of unit BB3 are mainly present in the northern part of the study area, concentrated as two sandbank deposits with occasional clay layers, located in between the infilled swales of unit BB2 (Fig. 9c). The deposition of unit BB3 is related to a mid-to-high-energy environment with sand remobilization, most likely due to re-establishment of tidal energy in the marine environment. Before and during deposition of unit BB3, erosion of underlying older units occurred leading to the formation of local undulating bounding surfaces. Erosion occurred in the southern part of the study area, where a 20 m-deep trough formed. This trough has a similar orientation and dimension as modern troughs present in the area, such as ‘Het Gat’ (Fig. 1b).

The mollusc assemblage, and the absence of arctic taxa, suggests generally warmer sea water conditions compared to underlying unit BB2, and a warming from sub-arctic to (cool) boreal conditions during deposition of unit BB3. Pollen are absent in the sandy facies within core BP050087 but might be present within thin clay-rich layers present in unit BB3 in other cores where the unit is thicker. The return of slightly warmer and higher-energy marine conditions reconstructed from the deposits of unit BB3 have been dated to 73–81.6 ka and is linked to Greenland Interstadial GI20 (Fig. 5).

4.5.4. Unit BB4 – correlated to late MIS 5a – earliest MIS 4 – GS20

Unit BB4 is divided in subunits BB4a and BB4b, which both indicate a westward progradation of sediments, filling the pre-existing underlying topography to the east of the Brown Bank Ridge (Fig. 9d). Unit BB4a is confined to the location of a trough present in the southern half of the study area, and has a different seismic facies compared to unit BB4b, which is more extensive. Based on the downlapping configuration of the stacked infill, the westward prograding sediments, or clinoforms, are interpreted to represent regressive pro-delta deposits (from the Rhine, based on the location and orientation, see sections 5.1 and 5.2) in a shallow marine environment. Units BB4a and BB4b are interpreted to represent a falling stage systems tract. As there are no sediment cores that have recovered unit BB4a (which was only deposited locally), its age, depth and composition are unknown. Unit BB4b consists of clay-rich sediments, representing a low-energy, shallow marine setting with high terrestrial input. The pollen and diatom assemblages from unit BB4b show that herb-rich open forests were present onshore, and the environment remained marine. Although the pollen and diatom content in unit BB4b has many similarities to unit BB2, the clay deposits of unit BB4b do not represent reworked sediments from unit BB2 as the pollen and diatom assemblages in both units have distinct differences. There are limited dates available from unit BB4b, with only one reliable quartz OSL date, suggesting deposition between 52 and 67 ka. The pollen

assemblage from unit BB4b however represents interstadial conditions, albeit slightly colder than the first part of BB2, which cannot be linked to the periglacial conditions of MIS 4. It should therefore be linked to either the end of MIS 5a or early MIS 3. Considering the similarities between the pollen and diatom content between unit BB4b and unit BB2, it is considered more likely that unit BB4b was also deposited under late MIS 5a conditions. This is supported by the fact the OSL ages from the clay-rich unit BB4b likely underestimate the true depositional age (see discussion in section 4.3.1). Support for a late MIS 5a age for unit BB4b comes from the concordant transition between unit BB3 and BB4, suggesting they likely formed shortly after one another. The OSL dates from overlying (post-BB) sediments in core BP050087 are not much younger than unit BB4b. The results suggest these overlying sediments were deposited during early MIS 3 or earlier, and that unit BB4 should be older. Considering all these lines of evidence, deposition of unit BB4 most likely occurred during GS20 (ca. 72 ka), although more future dating control is needed.

4.5.5. Overlying (Post-BB) deposits

In core BP050087, there is a 2.84 m thick succession (1.16–4 m) of sediments between unit BB4b and the Southern Bight Fm (see Fig. S4), consisting of very fine-grained sands (3–4 m), disturbed clays (2.1–3 m), and medium grey sands (1.16–2.1 m). The very fine-grained sands are laminated and match a transparent interval in the seismic data, which can be traced above surface H5, the latter being an irregular erosion surface formed throughout the study area (Fig. 3). This means that despite this transition is missing in the core, an unconformity is present between the fine-grained sands and underlying unit BB4b. One pollen-bearing sample (at 3.2 m) suggests cold conditions, with vegetation rich in grasses and herbs. Both fresh- and brackish water diatoms and marine molluscs occur within one interval in these sands (3.2 m). The overall character of the assemblage and mixed derivation make reworking from underlying Brown Bank deposits plausible. This is strengthened by the unconformity at the base of the fine-grained sands that links to erosion surface H5. However, the fine preservation characteristics of some of the molluscs and foraminifera may suggest the presence of marine conditions in this interval. We need larger sampling in future to ensure correct palaeoenvironmental interpretation for this mostly fine-grained interval.

The laminated clay interval overlying this very-fine sand interval shows disturbances and is linked to a locally present chaotic seismic interval above the previously mentioned transparent interval. This disturbance might be attributed to cryoturbation. The depositional environment of the clays is difficult to establish. Although the clays are barren in molluscs and diatoms, post depositional dissolution cannot be excluded. However, its high organic content makes deposition in a freshwater environment most likely. The pollen assemblage in this interval is warmer than the pollen assemblage of the underlying sand, containing about 50 % AP. An organic-rich interval filled with plant fibres has been radiocarbon dated to >40 ka (Table 4). Considering the increase in AP in combination with the luminescence dates, this clay was most likely deposited during early MIS 3. During temperate phases in MIS 3, dense tundra and steppe vegetation developed in most parts of NW Europe (Behre and Lade, 1986; Guiter et al., 2003), while temperate forest vegetation is reconstructed from multiple sites in the Eifel area (Britzius et al., 2024; Sirocko et al., 2016). The small amounts of thermophilous tree pollen in this interval may represent long-distance fluvial (Rhine) transport from the Eifel region.

Above the clay is an interval of grey, medium sand (1.16–2.1 m), and based on luminescence ages most likely corresponding to early MIS 3. The absence of pollen and diatoms and rare presence of molluscs limit the interpretation of the depositional environment, but the grain size, grain shape and laminations are suggestive of fluvial deposits linked to the presence of the Rhine, and can be assigned to the Kreftenheye Fm. More focus and detailed proxy work on these three deposits above the Brown Bank Fm might provide unprecedented details of landscape

development during a period of sea-level fall and sea floor emergence.

4.5.6. Intra unit comparisons

The four units of the Brown Bank Fm can be grouped in two consecutive cycles, consisting of units BB1–BB2 and units BB3–BB4 respectively. Both units BB1 and BB3 formed in cool-boreal environments with relatively high energy conditions allowing the formation of troughs and ridges. The main difference between the two cycles is that the underlying sea-floor topography was different at the onset of the two cycles. Below unit BB1 lies a regionally traceable and extensive erosional surface (H1), while the surface underneath unit BB3 formed due to more local processes. In addition, unit BB3 contains some clay layers while unit BB1 only consists of sands, indicating unit BB1 was deposited in higher energy conditions. During subsequent deposition of units BB2 and BB4, respectively, cooling and decreasing energy conditions occurred, which resulted in the infill of that swale-ridge topography.

There are multiple possible explanations for this change in energy. Changes in tidal energy are presumed the largest contribution, which can be affected by changes in water depth or changes in the basin geometry, both influenced by sea level. The proposed reduced connectivity at Dover Strait reduced circulation and current energy in the southern North Sea. In addition, it is likely that sea level varied a few meters between the deposition of the different BB-units. In the shallow marine conditions during deposition of the Brown Bank Fm, only a few meters of sea-level rise can change the environment from restricted to open marine (Eaton et al., 2020), increasing connectivity and circulation. We propose that sea level was slightly higher during deposition of unit BB1 and BB3 (Fig. 9a and c), enhancing open marine conditions with tidal currents. Subsequent sea-level lowering (Fig. 9b and d) resulted in a smaller marine basin with reduced circulation and tidal currents, resulting in clay deposition of units BB2 and BB4. However, it is also possible that the variations in energy occurred without changes in sea level. Delta progradation due to increased soil erosion during this time period also could have altered basin geometry and coastal palaeogeography. In addition, the depth of the storm wave base might have been deeper during deposition of units BB1 and BB3, resulting in higher energy conditions, and shallower during deposition of units BB2 and BB4. A shallow storm wave base may be the result of, amongst others, (seasonal) sea ice cover, or a smaller basin (which would be in combination with sea-level lowering). Although sea ice cover was not likely within the study area, given the absence of drop stones, sea ice cover in the central or northern North Sea would likely affect both the tidal regime and depth of the storm wave base in the southern North Sea.

5. Discussion

5.1. Palaeogeographic evolution of the southern North Sea region during the MIS 5a - MIS 4 transition

The new results on the extent and architecture of the Brown Bank Fm combined with new age constraints and environmental proxy data, provide new insights into the connectivity of the southern North Sea to the North Atlantic. These palaeoenvironmental results from the Brown Bank Fm, combined with reconstructions of the course of Rhine and Meuse and the position of their river mouths during the Early Glacial and Early Pleniglacial (Busschers et al., 2007; Hijma et al., 2012; Peeters et al., 2015), allow the palaeogeographic reconstruction of the response of shallow marine and terrestrial landscapes to the drastic cooling during the MIS 5-4 transition (Fig. 10).

During deposition of unit BB1, during MIS 5b and the start of MIS 5a, the southern North Sea was an open marine basin mainly influenced by tidal energy. The Rhine delta was positioned slightly further offshore compared to the current coastline due to lower sea levels, but delta activity did not directly impact our study area (Fig. 10a). As sea level continued to fall, regression likely resulted in narrowing of the English Channel and Dover Strait, limiting water exchange through the south

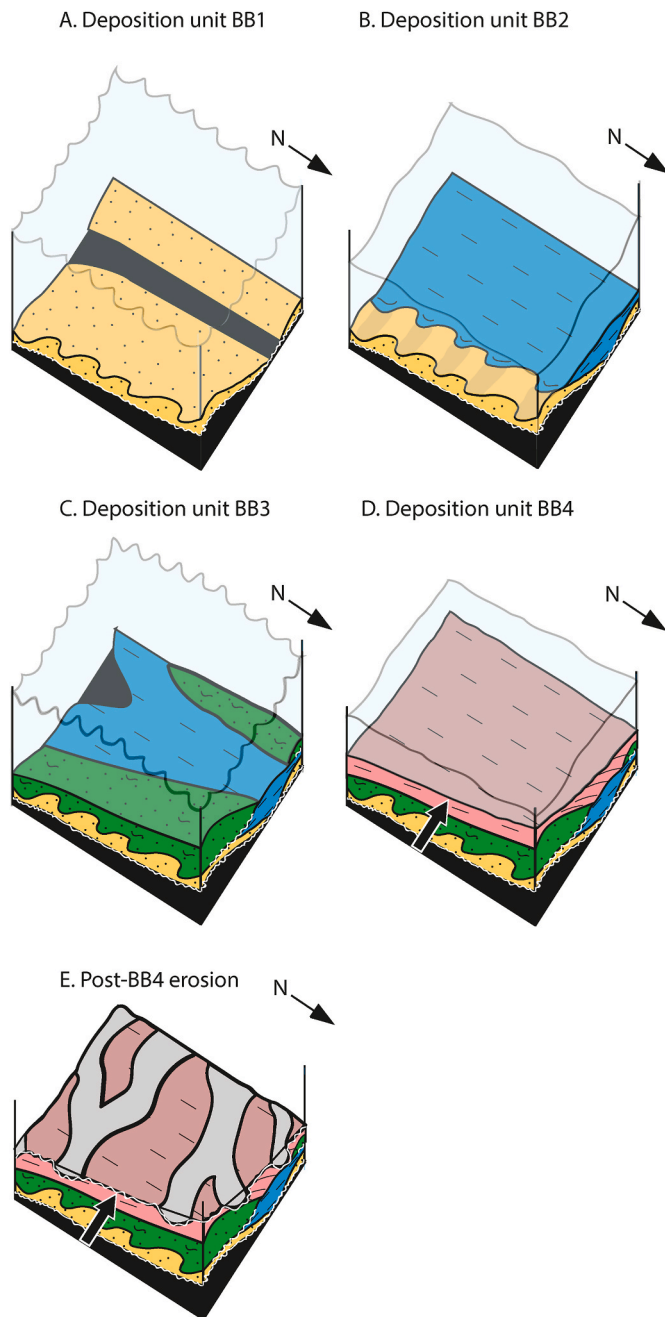


Fig. 9. Evolution of sedimentary units of the Brown Bank Fm. a) deposition of unit BB1 (yellow) in sand banks, with the simultaneous formation of troughs with non-deposition or erosion into the underlying, generally Middle Pleistocene, deposits (black). b) deposition of clay-rich unit BB2 (blue) draping and filling underlying topography. Sea level was likely slightly lower and there was less energy in the depositional environment. c) deposition of unit BB3 in sand banks, with simultaneous formation of troughs, especially in the southern part of the study area removing underlying BB-units and cutting into older deposits. Sea level was slightly higher than before with higher energy conditions. d) deposition of clay-rich unit BB4, consisting of prograding, pro-deltaic deposits with a source from the east (arrow). Sea level was low and there were low energy conditions. e) a braided river system eroding the top of unit BB4b during the MIS 4 sea-level lowstand. (For interpretation of the references to colour in this figure legend, the reader is referred to the Web version of this article.)

and allowing colder marine conditions to prevail in the southern North Sea.

During deposition of unit BB2, continued sea-level fall resulted in the

emergence of shallow parts of the sea floor. Progradation of the Rhine delta allowed pro-deltaic deposition in the study area. During deposition of unit BB2 bottom water hypoxia increased, related to increased stratification of the water column, while water temperatures decreased simultaneously. The combination of stratification and cooling can be explained by the presence of winter sea ice, which is most likely to occur when there was a further reduction, or complete shut-down of water exchange between the North Atlantic and the North Sea via the Dover Strait, as depicted in Fig. 10b. The deepest part of Dover Strait is currently below -50 m MSL, while the study area is on average approximately 30 m below MSL. Although the Dover Strait was likely less deeply eroded before the Last Glacial, it is unlikely that the Dover Strait was shallow enough to become fully subaerial while a marine environment persisted in the southern North Sea. It is, however, likely that Dover Strait became narrower, strongly reducing water exchange between the southern North Sea and the North Atlantic (Fig. 10b).

Such a disconnection from the North Atlantic at Dover Strait would lead to the formation of a marine embayment in the North Sea, where the only connection to the open ocean would be located towards the North, allowing cold water conditions (and arctic molluscs) to occur further south than might be expected based on the vegetation record onshore, comparable to today's Hudson Bay in Canada (Wesselingh et al., in prep).

During deposition of unit BB3, temporary warmer climate conditions would have resulted in warmer seawater temperatures within the entire North Sea. Warmer conditions do not necessarily require a re-connection at Dover Strait but instead can be the result of general warmer Atlantic water temperatures. Thus, water exchange at Dover Strait likely ceased during or directly after deposition of unit BB1 and did not recover until the Holocene.

During deposition of unit BB4, coastal regression and Rhine delta progradation resulted in clinoform deposition of pro-delta deposits within the marine environment. Unit BB4 was deposited in conditions that form the transition between the situations depicted in Fig. 10b and c. The pollen-based vegetation is temperate but resembles a more open woodland with increased dominance of grasses and herbs compared to unit BB2. Vegetation from MIS 4, based on Behre (1989); Britz et al. (2024); Helmens (2013), is not recorded in the Brown Bank Fm. The top of the Brown Bank Fm (surface H5) is currently present between -32 and -46 m below sea level (LAT). When corrected for the average subsidence rates in the North Sea basin over the past 75 ka, the highest elevation of the top of the Brown Bank Fm was situated around -23 m below sea level (Fig. 2d; based on Cohen et al., 2022). This is a first order correction, ignoring glacio-isostatic effects, and provides only an indication of the amount of subsidence of the basin floor. It does mean that sea level remained relatively high during deposition of the entire Brown Bank Fm (above this approximated -23 m), and small changes in sea level largely influenced the depositional environment (section 4.5 and Eaton et al., 2020). Around 72 ka, when the North Sea became exposed, regional sea level dropped below approximately -23 m. This sea level is higher compared to reconstructions of global mean sea level of Spratt and Lisiecki (2016), and similar to the reconstruction of Gowan et al. (2021) (Fig. 1).

The limited sand input into the southern North Sea during cold periods (unit BB2 and BB4) may have been the result of increased sand deposition within the channel belts onshore. Sand deposition in channel belts is common in braided river systems during the cold periods (Gouw and Erkens, 2007), which might have occurred onshore during deposition of units BB2 and BB4. Relatively more sand was transported towards the North Sea in warmer periods (deposition units BB1 and BB3), when rivers might have had more meandering trajectories.

5.2. Palaeogeographic evolution of the southern North Sea region during MIS 4 and early MIS 3

The widespread erosional surface H5, the upper bounding surface of

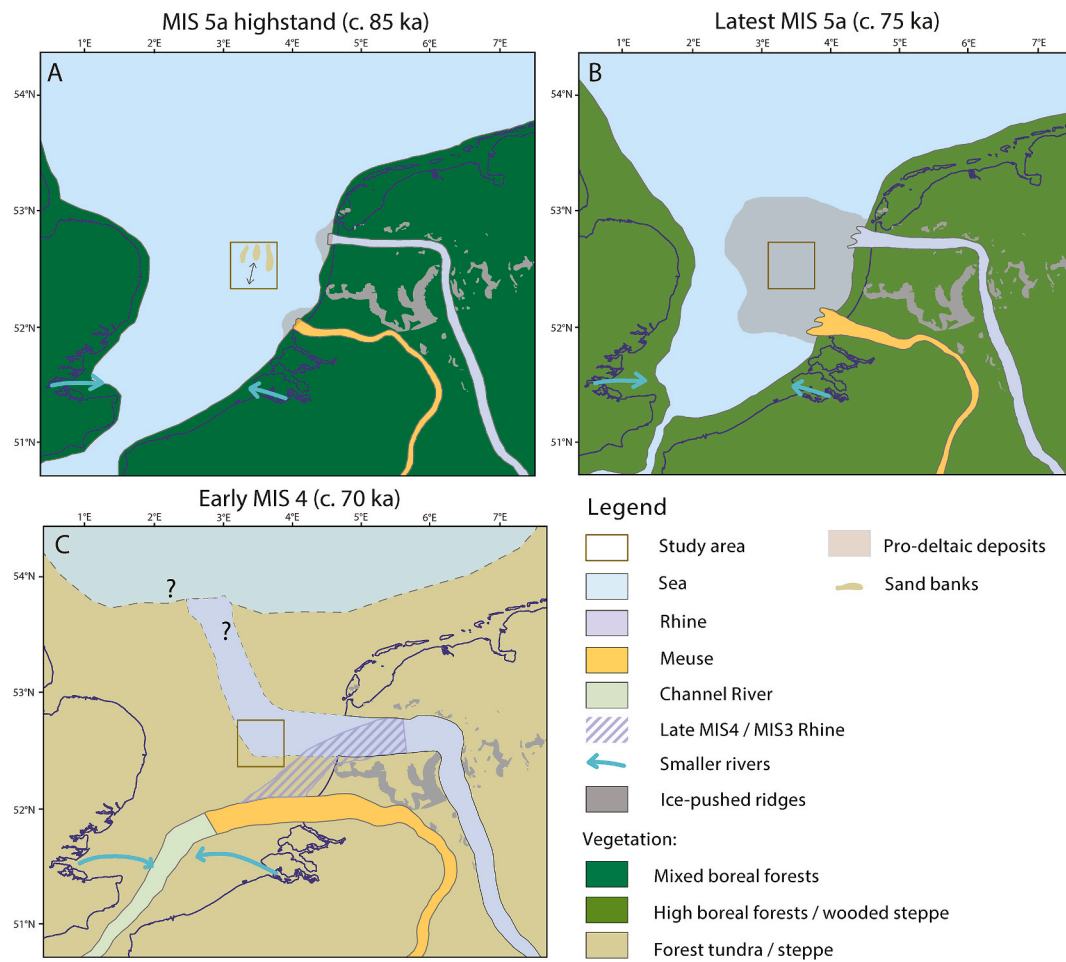


Fig. 10. Palaeogeographic evolution of the southern North Sea area focusing on the fluvial and coastal evolution during the MIS 5a-4 transition. Vegetation is generalized for the entire region, and the channel belts of the Rhine and Meuse rivers are shown, based on [Busschers et al. \(2007\)](#), [Hijma et al. \(2012\)](#) and [Peeters et al. \(2015\)](#). The modern coastline and study area are shown for reference. A) Highstand phase of MIS 5a, with sand banks in the study area, arrows indicating the approximate current direction. B) Latest phase of MIS 5a, where fine-grained pro-deltaic deposits spread over large areas of the southern North Sea, and C) Early MIS 4, where the wide channel belts represent the extension of the braided river systems. The hatched area represents fluvial deposits of the Rhine from late MIS 4 and/or MIS 3, showing that the Rhine shifted towards the south during or after MIS 4. The position of the coastline and Rhine delta are dashed as the exact location is unknown due to the fast regression of the North Sea during this period.

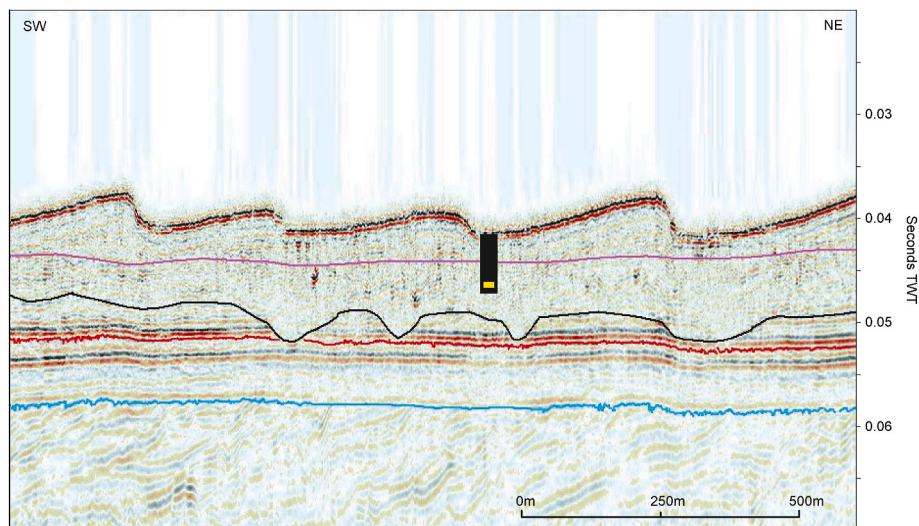


Fig. 11. Example of a north-south seismic profile in wind farm IJV (line 0273-P193), where a similar base (H1, blue) and top (H5, black) of the Brown Bank Fm are observed. The location of cove IJV501-VC is shown in black, with the depth of the OSL sample indicated by a yellow square. Retrieved from ([GEOxyz, 2021](#), appendices). (For interpretation of the references to colour in this figure legend, the reader is referred to the Web version of this article.)

subunits BB4a and BB4b, can be traced into wind farms IJV and HKW, where this erosional surface displays the same irregular character (Fig. 11, GEOxyz, 2021; Periplus Archeomare, 2023). In IJV, this erosional horizon (defined as the 'base of unit B') has been mapped and interpreted as a braided river plain, which incises the top of the Brown Bank Fm (Periplus Archeomare, 2023). The character of this surface changes towards the north, becoming flatter and shallower (Periplus Archeomare, 2023a), providing a northern limit for the braided river plain (Periplus Archeomare, 2023; Fig. 10c). Currently, one OSL date was obtained for the very fine sand interval directly above unit BB4b in our dataset (core BP050087; 52.6–63.6 ka, Fig. 8), one date from the medium grained sand higher in that core (BP050087; 49.9–55.9 ka, Fig. 8) and one in IJV located ca. 10 km north of our study site (IJV501-VC; 65.3–72.7 ka), suggesting an age of MIS 4 and early MIS 3. The location of this braided river plain might have shifted through the area over time, leading to an extensive heterochronic erosional surface. This erosional surface indicates a relative drop in sea level across the area after the deposition of the Brown Bank Fm, and erosion of the top of the Brown Bank Fm by fluvial activity during a sea-level lowstand (Fig. 9e). While most sediments above the Brown Bank Fm likely have a fluvial origin, a presumed fresh-brackish submerged environment (possibly lagoonal or even shallow marine) was present during deposition of the clay in core BP050087 (2–3 m, Fig. 8). More study is needed on the sediments overlying unit BB4b to better understand the array of palaeoenvironments which existed after sea floor emergence.

The NW-SE orientation of this braided river plain, as well as the extensive area covered, point to a connection to the Rhine river, which is the largest river in the southern North Sea area (Fig. 10c). In addition, the clinoforms observed in the westward progradation of unit BB4 are likely shaped by the prograding Rhine delta before emergence. Provenance studies are needed to confirm the correlation to the Rhine. The sedimentary characteristics of the fluvial sediment observed in core BP050087 (1.16–2.1 m) and in IJV501-VC closely correlate to sedimentary units A4 and A5 onshore (Busschers et al., 2007; Peeters et al., 2016). This correlation of sediments above the Brown Bank Fm to the Rhine means that it must have headed west over the exposed former sea floor and most probably drained towards the north during the first part of MIS 4 (Fig. 10c). Either towards the end of MIS 4 or during MIS 3, the Rhine shifted to the south (Busschers et al., 2007; Peeters et al., 2015) (shaded region in Fig. 10c). The Brown Bank Fm was likely more widespread than the current distribution, as in some parts the fluvial deposits clearly cut into its deposits. To the southeast of the Brown Bank region, small patches of the Brown Bank Fm are preserved, which might be remnants of a more extensive distribution (Garritsen, 2024).

The proposed northerly route of the Rhine suggests that it did not drain to the Channel River during early MIS 4 (Fig. 10). The Channel River is a mega-river system that drained western Europe and the parts of the European Ice Sheet and flowed into the Atlantic at the Bay of Biscay during the sea-level lowstand of the last glacial cycle (e.g. Gibbard, 1995; Toucanne et al., 2023). Multiple cores from the deep Bay of Biscay (MD95-2002, MD13-3438, MD03-2692; Fig. 1) contain abyssal fan sediments fed by the Channel River. Based on ϵNd values, Toucanne et al. (2023) argue that the Channel River did not drain the North European plain or Baltic Shield during MIS 4, and suggests that central European rivers, including the Rhine, discharged northwards, in contrast to MIS 2 (Ménot et al., 2006; Toucanne et al., 2023). This is in line with the braided river patterns of early MIS 4 age that have been found on top of the Brown Bank Fm and our reconstruction presented in Fig. 10c. The data of Toucanne et al. (2023) indicate that this northward routing of the Rhine river must have persisted throughout the entire MIS 4.

5.3. Comparison to previous work

Waajen et al., 2024b described a window of sediment preservation in the southern North Sea capturing sediments of the MIS 5a-MIS 4

transition, which represents one of the largest climate transitions of the last glacial cycle. The low-energy marine conditions with a high sediment influx allowed significant amounts of clay deposition within a fairly short time period. The new results from this study provide high-resolution data on the sedimentary architecture and environmental evolution during this falling stage systems tract, capturing the stepwise transition of the last glacial inception in unprecedented detail. Although fluvial activity eroded the top of unit BB4b in most places, fluvial deposits also covered the Brown Bank Fm and protected it from erosion during the Holocene transgression.

Previously, the Brown Bank Fm has been interpreted to reflect a lagoonal to freshwater system (e.g. Cameron et al., 1989; Zagwijn, 1983). In addition, Zagwijn (1983) suggested, based on pollen and ostracod data, that this freshening of the southern North Sea occurred during pollen zone EW1a, which is the first pollen zone of the Early Weichselian (related to the Herning stadial; MIS 5d). Zagwijn's core P5-4 is located at the northern end of our study area (ca. 5 km northwest of core BP050087, Fig. 1b), in the vicinity of clay units BB2 and BB4b. The pollen assemblage assigned to pollen zone EW1a in core P5-4 is similar to pollen zones PZ-C and PZ-D identified in this study, although the concentration of grasses resembles PZ-E. The new data presented in our study do not provide evidence of clay deposition in the Early Weichselian within this region and therefore indicate that this correlation to the Herning stadial is likely incorrect. Based on our data, a lagoonal or freshwater system only occurred after deposition of unit BB4, when the westward progradational patterns suggest regression. Indeed, the increase in freshwater diatoms within core BP050087 occurs in the sandy deposits above unit BB4b, corresponding to the deposits above the regional erosional surface (H5). However, as discussed in section 4.5, marine influence cannot be ruled out due to the presence of some well-preserved marine molluscs.

Different subunits have been identified in the Brown Bank Fm before. Wessex Archaeology (2018) and Eaton et al. (2020) described a subdivision between the Upper and Lower Brown Bank Fm within the Norfolk Vanguard wind farm area in UK waters. There, the Lower Brown Bank Fm, linked to MIS 5e-d, was combined with the Eem Formation and comprises silty sands, whereas the Upper Brown Bank Fm, linked to MIS 5d-MIS 3, consists of clayey silty sands infilling channels. We present a more detailed subdivision of the Brown Bank Fm, based on a detailed multiproxy analysis from Dutch waters. Although the Norfolk Vanguard wind farm is located ca. 30 km west of the study area, we correlate the Lower Brown Bank Fm with unit BB1, while units BB2, BB3 and BB4 may be attributed to the Upper Brown Bank Fm. The accepted OSL ages of the Upper Brown Bank Fm in Norfolk Vanguard windfarm area (Wessex Archaeology, 2018) provide a range between 50.8 and 90.9, very similar to the age ranges provided in this manuscript. The high equivalent doses could be an indication that also in this area, saturation may affect the age results. The similarity in ages suggests synchronicity of deposition of the Brown Bank Fm in a larger region, although the large range does not exclude asynchronicity. In wind farm zones Hollandse Kust West (HKW) and IJmuiden Ver (IJV; Fig. 1b), nearby our study area, similar variations in seismic facies as described in this study can be discerned within the Brown Bank Fm (Fugro, 2019; GEOxyz, 2021), indicating that our proposed subdivision into four units might be extended beyond our study area (Fig. 11). This may indicate a regional forcing on the depositional environment, rather than local variations. The marine depositional environment reconstructed for all units of the Brown Bank Fm is additionally supported by foraminifera data from the Brown Bank Fm found in the IJV wind farm, north of our study area, where subtidal marine taxa (containing several species of *Bolivina*, *Elphidium*, *Haynesina* and *Cassidulina*) are the most abundant foraminifera, suggesting water depth <30 m (Periplus Archeomare, 2023). This variety in seismic facies is mainly present in this marginal region of deposition of the Brown Bank Fm, while west of the Brown Bank ridge the Brown Bank Fm resembles a thick pack of laminated sediment up to 10 m thick, which is more the typical seismic signature of the Brown Bank Fm as described in

literature (e.g. Cameron et al., 1989). It seems that closer to the palaeo-coastline, palaeoenvironmental changes were larger compared to locations further offshore, resulting in the stack of BB units in this region.

6. Conclusions

The sediments of the Brown Bank Formation recording the MIS 5–MIS 4 transition in the southern North Sea provide insights into the depositional system changes and the palaeogeographic evolution of the area, through a major climate transition with successive severe cooling events. Our new data show that the thick and widespread deposit of the Brown Bank Fm can be divided into four seismic facies (unit BB1 – BB4) and consist of seven characterised lithofacies (LF1–LF7). Multi-proxy results show that these units were deposited in alternating energy regimes in a shallow, but open marine depositional environment. Two cooling phases are observed (within units BB2 and BB4), while units BB1 and BB3 represent slightly warmer conditions. The entire Brown Bank Fm was deposited during the relatively short time period corresponding to the transition from MIS 5 to 4, indicating a significant sediment supply from land which was trapped in this part of the southern North Sea. The new results provide additional insights into the heterogeneity and distribution of the different units but also allow detailed characterisation of the terrestrial landscape and the only slight opening of the vegetation. The proposed link to the NGRIP record allows us to assign the time that this part of the southern North Sea became exposed, most likely around 72 ka, with much higher detail than OSL-dates alone would provide. The climate fluctuations recorded in the NGRIP core thus strongly influenced the landscape changes in the southern North Sea.

CRediT authorship contribution statement

Irene Waajen-Labee: Conceptualization, Methodology, Formal analysis, Investigation, Project administration, Writing – original draft, Writing – review & editing, Visualization. **Ruth Plets:** Conceptualization, Formal analysis, Investigation, Writing – original draft, Writing – review & editing, Visualization. **Víctor Cartelle:** Conceptualization, Writing – review & editing. **Marieke Cuperus:** Investigation. **Timme Donders:** Conceptualization, Project administration, Writing – review & editing, Supervision. **Sytze van Heteren:** Conceptualization, Writing – review & editing. **Thomas Mestdag:** Conceptualization, Formal analysis, Writing – review & editing. **Friederike Wagner-Cremer:** Project administration, Writing – review & editing, Supervision. **Jakob Wallinga:** Formal analysis, Validation, Investigation, Writing – review & editing. **Frank Wesselingh:** Conceptualization, Investigation, Writing – review & editing. **Freerk Busschers:** Conceptualization, Project administration, Writing – review & editing, Supervision.

Declaration of competing interest

The authors declare that they have no known competing financial interests or personal relationships that could have appeared to influence the work reported in this paper.

Acknowledgements

This work was funded by TNO – Geological Survey of the Netherlands and a grant from the Cultural heritage Agency of the Netherlands (project VER-SKAN, number 126958). We acknowledge the contribution of Fugro, and Sven Plasman in particular, for placing core BP050087, which greatly improved the dataset and our understanding of the Brown Bank Fm. We thank Aleksandra Cvetkoska and Geurt Verweij from Waardenburg Ecology for providing diatom analyses on core BP050087, and Frans Bunnik for analysing half of the pollen samples. We would like to thank the staff of the luminescence laboratories at

the Netherlands Centre for Luminescence Dating and at the School of Earth and Environmental Sciences for their luminescence measurements, and Tim Kinnaird for providing his insights on the luminescence results. We would like to thank the captain and crew, and everyone who helped on board of the RV *Pelagia* and RV *Simon Stevin* – without their effort and patience, we would not have been able to acquire such large amount of data. Special thanks to Tine Missiaen for her continual support and guidance. We thank the Royal Netherlands Institute for Sea Research (NIOZ), and Rick Hennekam in particular, for assisting with XRF data acquisition and interpretation. We thank the Netherlands Enterprise Agency (RVO) for providing the all sub-bottom data from the wind farm zones free of charge, licensed under Creative Commons 4.0 CC-BY-SA.

Appendix A. Supplementary data

Supplementary data to this article can be found online at <https://doi.org/10.1016/j.quascirev.2025.109442>.

Data availability

Palynological, diatom and XRF data are available in the Neotoma database.

References

- Barlow, N.L.M., Shennan, I., Long, A.J., Gehrels, W.R., Saher, M.H., Woodroffe, S.A., Hillier, C., 2013. Salt marshes as late holocene tide gauges. *Global Planet. Change* 106, 90–110. <https://doi.org/10.1016/j.gloplacha.2013.03.003>.
- Batchelor, C.L., Margold, M., Krapp, M., Murton, D.K., Dalton, A.S., Gibbard, P.L., Stokes, C.R., Murton, J.B., Manica, A., 2019. The configuration of Northern Hemisphere ice sheets through the Quaternary. *Nat. Commun.* 10 (1), 1–10. <https://doi.org/10.1038/s41467-019-11601-2>.
- Behre, K.-E., Lade, U., 1986. Eine Folge von Eem und 4 Weichsel-Interstadialen in Oerel/Niedersachsen und ihr Vegetationsablauf. *E&G Quaternary Science Journal* 36 (1), 11–36. <https://doi.org/10.3285/eg.36.1.02>, 1986.
- Behre, K.E., 1989. Biostratigraphy of the last glacial period in Europe. *Quat. Sci. Rev.* 8 (1), 25–44. [https://doi.org/10.1016/0277-3791\(89\)90019-X](https://doi.org/10.1016/0277-3791(89)90019-X).
- Britz, S., Dreher, F., Maisel, P., Sirocko, F., 2024. Vegetation patterns during the last 132,000 Years : a synthesis from twelve Eifel maar sediment cores (Germany): the ELSA-23-pollen-stack. *Quaternary* 7 (8). <https://doi.org/10.3390/quat7010008>.
- Busschers, F.S., Kasse, C., van Balen, R.T., Vandenbergh, J., Cohen, K.M., Weerts, H.J.T., Wallinga, J., Johns, C., Cleveringa, P., Bunnik, F.P.M., 2007. Late Pleistocene evolution of the Rhine-Meuse system in the southern North Sea basin: imprints of climate change, sea-level oscillation and glacio-isostasy. *Quat. Sci. Rev.* 26 (25–28), 3216–3248. <https://doi.org/10.1016/j.quascirev.2007.07.013>.
- Cain, S.A., 1939. Pollen analysis as a paleo-ecological research method. *Bot. Rev.* 5, 627–654.
- Cameron, T.D.J., Crosby, A., Balson, P.S., Jeffery, D.H., Lott, G.K., Bulat, J., Harrison, D.J., 1992. United Kingdom Offshore Regional Report: the Geology of the Southern North Sea. HMSO for the British Geological Survey.
- Cameron, T.D.J., Schuttenhelm, R.T.E., Laban, C., 1989. Middle and upper Pleistocene and holocene stratigraphy in the southern North Sea between 52° and 54°N, 2° to 4°E. In: Henriot, J.P., De Moor, G. (Eds.), *The Quaternary and Tertiary Geology of the Southern Bight, North Sea*. Ministry of Economic Affairs - Belgian Geological Survey, pp. 119–136.
- Cartelle, V., Barlow, N.L.M., Hodgson, D.M., Busschers, F.S., Cohen, K.M., Meijninger, B.M.L., Van Kesteren, W.P., 2021. Sedimentary architecture and landforms of the late Saalian (MIS 6) ice sheet margin offshore of The Netherlands. *Earth Surf. Dyn.* 9 (6), 1399–1421. <https://doi.org/10.5194/esurf-9-1399-2021>.
- Cattaneo, A., Steel, R.J., 2003. Transgressive deposits: a review of their variability. *Earth-Sci. Rev.* 62 (3–4), 187–228. [https://doi.org/10.1016/S0012-8252\(02\)00134-4](https://doi.org/10.1016/S0012-8252(02)00134-4).
- Catuneanu, O., 2022. *Principles of Sequence Stratigraphy*, second ed. Elsevier. <https://doi.org/10.1016/b978-0-444-53353-1.01001-4>.
- Cohen, K.M., Cartelle, V., Barnett, R., Busschers, F.S., Barlow, N.L.M., 2022. Last interglacial sea-level data points from northwest Europe. *Earth Syst. Sci. Data* 14, 2895–2937. <https://doi.org/10.5194/essd-2021-390>.
- Cvetkoska, A., Levkov, Z., Reed, J., 2012. Reconstructing Holocene environmental change in Lake Ohrid (Macedonia/Albania) using diatom as proxies. *Maced. J. Ecol. Environ.* 14 (1–2), 7–18. <https://doi.org/10.59194/MJEE12141-207c>.
- Cvetkoska, A., Verweij, G.L., 2024. Resultaten Analyse bodemonsters van project De Bruine Bank, report Waardenburg Ecology.
- De Clercq, M., Missiaen, T., Wallinga, J., Zurita Hurtado, O., Versendaal, A., Mathys, M., De Batist, M., 2018. A well-preserved eemian incised-valley fill in the southern North Sea basin, Belgian continental shelf - coastal plain: implications for northwest European landscape evolution. *Earth Surf. Process. Landf.* 43 (9), 1913–1942. <https://doi.org/10.1002/esp.4365>.

- Denys, L., 1999. A diatom and radiocarbon perspective of the palaeoenvironmental history and stratigraphy of Holocene deposits between Oostende and Nieuwpoort (Western Coastal Plain, Belgium). *Geol. Belg.* 2 (3–4), 111–140. <https://doi.org/10.20341/gb.2014.014>.
- Eaton, S.J., Hodgson, D.M., Barlow, N.L.M., Mortimer, E.E.J., Mellett, C.L., 2020. Palaeogeographical changes in response to glacial–interglacial cycles, as recorded in Middle and Late Pleistocene seismic stratigraphy, southern North Sea. *J. Quat. Sci.* 35 (6), 760–775. <https://doi.org/10.1002/jqs.3230>.
- Emery, A.R., Hodgson, D.M., Barlow, N.L.M., Carrivick, J.L., Cotterill, C.J., Mellett, C.L., Booth, A.D., 2019a. Topographic and hydrodynamic controls on barrier retreat and preservation: an example from Dogger Bank, North Sea. *Mar. Geol.* 416 (December 2018), 105981. <https://doi.org/10.1016/j.margeo.2019.105981>.
- Emery, A.R., Hodgson, D.M., Barlow, N.L.M., Carrivick, J.L., Cotterill, C.J., Phillips, E., 2019b. Left high and dry: deglaciation of dogger bank, North Sea, recorded in proglacial lake evolution. *Front. Earth Sci.* 7 (September), 1–27. <https://doi.org/10.3389/feart.2019.00234>.
- Faegri, K., Kaland, P.E., Krywinski, K., 1989. Textbook of Pollen Analysis, fourth ed. John Wiley & Sons <https://www.cabdirect.org/cabdirect/abstract/19930670810>.
- Fugro, 2019. Geophysical Results Report: Hollandse Kust (West) Wind Farm Zone Survey 2018.
- Garritsen, A., 2024. Stratigraphic correlation and depositional setting of the Early Weichselian (MIS 5d-a) sediments and surrounding Pleistocene and Holocene sediments in the Dutch Offshore. Southern North Sea; A Regional Perspective from Seismic Interpretation and Sediment. Utrecht University.
- GEOSYZ, 2021. Geophysical Survey - IJmuiden Ver Wind Farm Zone (Site I - IV) (Issue November).
- Gibbard, P.L., 1995. The formation of the strait of dover. *Geol. Soc. Spec. Publ.* 96 (96), 15–26. <https://doi.org/10.1144/GSL.SP.1995.096.01.03>.
- Gouw, M.J.P., Erkens, G., 2007. Architecture of the Holocene Rhine-Meuse delta (The Netherlands) - a result of changing external controls. *Neth. J. Geosci.* 86 (1), 23–54.
- Gowan, E.J., Zhang, X., Khosravi, S., Rovere, A., Stocchi, P., Hughes, A.L.C., Gyllencreutz, R., Mangerud, J., Svendsen, J., Lohmann, G., 2021. A new global ice sheet reconstruction for the past 80000 years. *Nat. Commun.* 12 (1199), 1–9. <https://doi.org/10.1038/s41467-021-21469-w>.
- Guiter, F., Andrieu-Ponel, V., de Beaulieu, J.L., Cheddadi, R., Calvez, M., Ponel, P., Reille, M., Keller, T., Goeury, C., 2003. The last climatic cycles in Western Europe: a comparison between long continuous lacustrine sequences from France and other terrestrial records. *Quat. Int.* 111 (1), 59–74. [https://doi.org/10.1016/S1040-6182\(03\)00015-6](https://doi.org/10.1016/S1040-6182(03)00015-6).
- Head, M.J., Gibbard, P.L., 2015. Early-Middle Pleistocene transitions: linking terrestrial and marine realms. *Quat. Int.* 389, 7–46. <https://doi.org/10.1016/j.quaint.2015.09.042>.
- Helmens, K.F., 2013. The Last Interglacial-Glacial Cycle (MIS 5-2) Re-examined Based on Long Proxy Records from Central and Northern Europe (Issue October).
- Hennekam, R., de Lange, G., 2012. X-ray fluorescence core scanning of wet marine sediments: methods to improve quality and reproducibility of high-resolution paleoenvironmental records. *Limnol. Oceanogr. Methods* 10 (12), 991–1003. <https://doi.org/10.4319/lom.2012.10.991>.
- Hijma, M.P., Cohen, K.M., Roebroeks, W., Westerhoff, W.E., Busschers, F.S., 2012. Pleistocene Rhine–Thames landscapes: geological background for hominin occupation of the southern North Sea region. *J. Quat. Sci.* 27 (1), 17–39. <https://doi.org/10.1002/jqs.1549>.
- Huijzer, B., Vandenbergh, J., 1998. Climatic reconstruction of the weichselian pleniglacial in northwestern and central Europe. *J. Quat. Sci.* 13 (5), 391–417. [https://doi.org/10.1002/\(SICI\)1099-1417\(199809\)13:5<391::AID-JQS397>3.0.CO;2-6](https://doi.org/10.1002/(SICI)1099-1417(199809)13:5<391::AID-JQS397>3.0.CO;2-6).
- Jansen, F.J.H., Weering, T.C.E., Eisma, D., 1979. Late quaternary sedimentation in the eastern Mediterranean sea. In: Oele, E., Schüttenhelm, R.T.E., Wiggers, A.J. (Eds.), *The Quaternary History of the North Sea*. Acta Univ. Ups. Symp. Univ. Ups. Annum Quingentesimum Celebrantis, pp. 175–187. Issue December.
- Joon, B., Laban, C., Van der Meer, J.J.M., 1990. The Saalian glaciation in the Dutch part of the North sea. *Geol. Mijnbouw* 69 (2), 151–158.
- Kidwell, S.M., 1986. Models for fossil concentrations : paleobiologic implications. *Paleobiology* 12 (1), 6–24.
- Kooi, H., Johnston, P., Lambeck, K., Smither, C., Molendijk, R., 1998. Geological causes of recent (~ 100 yr) vertical land movement in the Netherlands. *Tectonophysics* 299 (4), 297–316.
- Lamb, R.M., Harding, R., Huuse, M., Stewart, M., Brocklehurst, S.H., 2018. The early quaternary north sea basin. *J. Geol. Soc.* 175 (2), 275–290. <https://doi.org/10.1144/jgs2017-057>.
- Limpenny, S.E., Barrio Fróján, C., Cotterill, C., Foster-Smith, R.L., Pearce, B., Tizzard, L., Limpenny, D.L., Long, D., Walmsley, S., Kirby, S., Baker, K., Meadows, W.J., Rees, J., Hill, J., Wilson, C., Leivers, M., Churchley, S., Russell, J., Birchenough, A.C., et al., 2011. The East coast regional environmental characterisation. In: Cefas Open Report 08/04. MEPP.
- Martin-Puertas, C., Tjallingii, R., Bloemsa, M., Brauer, A., 2017. Varved sediment responses to early Holocene climate and environmental changes in Lake Meerfelder Maar (Germany) obtained from multivariate analyses of micro X-ray fluorescence core scanning data. *J. Quat. Sci.* 32 (3), 427–436. <https://doi.org/10.1002/jqs.2935>.
- McGuire, A.M., 2020. Resolving abrupt palaeoenvironmental changes in a lake sediment sequence from Ioannina, northwest Greece. Doctoral dissertation. University of Cambridge, England.
- Ménnot, G., Bard, E., Rostek, F., Weijers, J.W.H., Hopmans, E.C., Scheuten, S., Sinninghe Damsté, J.S., 2006. Early reactivation of European rivers during the last deglaciation. *Science* 313 (5793), 1623–1625. <https://doi.org/10.1126/science.1130511>.
- Mitchum, R.M.J., Vail, P.R., Samgree, J.B., 1977. Seismic stratigraphy and global changes of sea level, Part 6: stratigraphic interpretation of seismic reflections patterns in depositional sequences. In: Payton, C.E. (Ed.), *Seismic Stratigraphy – Applications to Hydrocarbon Exploration*, 26. American Association of Petroleum Geologists Memoir (pp. 177–133).
- Mitchum, R.M., Vail, P.R., 1977. Seismic stratigraphy and global changes of sea level, Part 7: seismic stratigraphic interpretation procedure. In: Payton, C.E. (Ed.), *Seismic Stratigraphy – Applications to Hydrocarbon Exploration*, 26. American Association of Petroleum Geologists Memoir, pp. 135–144.
- Moreau, J., Huuse, M., Janszen, A., van der Vegt, P., Gibbard, P.L., Moscardello, A., 2012. The glaciogenic unconformity of the southern North Sea. *Glaciogenic Reservoirs and Hydrocarbon Systems* 368, 99–110.
- Narayana, Y., Rajashekara, K.M., 2010. The importance of physico-chemical parameters on the speciation of natural radionuclides in riverine ecosystems. *J. Environ. Radioact.* 101 (11), 958–964. <https://doi.org/10.1016/j.jenvrad.2010.06.015>.
- North Greenland Ice Core Project (NGRIP) Members, 2004. High-resolution record of Northern Hemisphere climate extending into the last interglacial period. *Nature* 431 (7005), 147–151. www.nature.com/nature.
- Oele, E., 1971. The Quaternary geology of the southern area of the Dutch part of the North Sea. *Geol. Mijnbouw* 50 (3), 461–474.
- Peeters, J., Busschers, F.S., Stouthamer, E., 2015. Fluvial evolution of the Rhine during the last interglacial-glacial cycle in the southern North Sea basin: a review and look forward. *Quat. Int.* 357, 176–188. <https://doi.org/10.1016/j.quaint.2014.03.024>.
- Peeters, J., Busschers, F.S., Stouthamer, E., Bosch, J.H.A., Van den Berg, M.W., Wallinga, J., Versendaal, A.J., Bunick, F.P.M., Middelkoop, H., 2016. Sedimentary architecture and chronostratigraphy of a late Quaternary incised-valley fill: a case study of the late Middle and Late Pleistocene Rhine system in The Netherlands. *Quat. Sci. Rev.* 131, 211–236. <https://doi.org/10.1016/j.quascirev.2015.10.015>.
- Periplus Archaeomare, 2023. Archaeological Assessment of Geophysical Survey results. IJmuiden Ver Gamma.
- Periplus Archaeomare, 2023. Archaeological Assessment of Paleolandscapes. IJmuiden Ver Alpha and Beta.
- Ribeiro, L., Benyoucef, I., Poulin, M., Jesus, B., Rosa, P., Méléder, V., Du, G.Y., Barillé, L., 2021. Spatio-temporal variation of microphytobenthos biomass, diversity and assemblage structure in the Loire Estuary, France. *Aquat. Microb. Ecol.* 87, 61–77. <https://doi.org/10.3354/AME01971>.
- Rothwell, R.G., Croudace, I.W., 2015. Twenty years of XRF core scanning marine sediments: What do geochemical proxies tell us? *Micro-XRF Stud. Sediment Cores: Appl. Non-destr. Tool Environ. Sci.* 25–102. https://doi.org/10.1007/978-94-017-9849-5_2.
- Sánchez Goñi, M.F., Bard, E., Landais, A., Rossignol, L., D'errico, F., 2013. Air-sea temperature decoupling in western Europe during the last interglacial-glacial transition. *Nat. Geosci.* 6 (10), 837–841. <https://doi.org/10.1038/ngeo1924>.
- Schimanski, A., Statteger, K., 2005. Deglacial and Holocene evolution of the Vietnam shelf: stratigraphy, sediments and sea-level change. *Mar. Geol.* 214 (4), 365–387. <https://doi.org/10.1016/j.margeo.2004.11.001>.
- Seppä, H., Bennett, K.D., 2003. Quaternary pollen analysis: recent progress in palaeoecology and palaeoclimatology. *Prog. Phys. Geogr.* 27 (4), 548–579. <https://doi.org/10.1191/0309133303pp3940a>.
- Shennan, I., Lambeck, K., Flather, R., Horton, B., McArthur, J., Innes, J., Lloyd, J., Rutherford, M., Wingfield, R., 2000. Modelling western North Sea palaeogeographies and tidal changes during the Holocene. Geological Society, London, Special Publication 166, 299–319. <https://doi.org/10.1144/GSL.SP.2000.166.01.15>.
- Sirocko, F., Knapp, H., Dreher, F., Förster, M.W., Albert, J., Brunck, H., Veres, D., Dietrich, S., Zech, M., Hambach, U., Röhner, M., Rudert, S., Schwibus, K., Adams, C., Sigl, P., 2016. The ELSA-Vegetation-Stack: reconstruction of Landscape Evolution Zones (LEZ) from laminated Eifel maar sediments of the last 60,000 years. *Global Planet. Change* 142, 108–135. <https://doi.org/10.1016/j.gloplacha.2016.03.005>.
- Spratt, R.M., Lisiecki, L.E., 2016. A Late Pleistocene sea level stack. *Clim. Past* 12 (4), 1079–1092. <https://doi.org/10.5194/cp-12-1079-2016>.
- Ten Veen, Vis, G.J., De Jager, J., Wong, T.E. (Eds.), 2025. *Geology of the Netherlands*, second ed. Amsterdam University Press.
- Toucanne, S., Rodrigues, T., Menot, G., Soulet, G., Cheron, S., Billy, I., Eynaud, F., Antoine, P., Sinninghe Damsté, J.S., Bard, E., Sanchez Goñi, M.F., 2023. Marine isotope stage 4 (71–57 ka) on the western European margin: insights to the drainage and dynamics of the western European ice sheet. *Global Planet. Change* 229 (August). <https://doi.org/10.1016/j.gloplacha.2023.104221>.
- Velenturf, A.P.M., Emery, A.R., Hodgson, D.M., Barlow, N.L.M., Mohtaj Khorasani, Van Alstine, J., Peterson, E.L., Piazzolo, S., Thorp, M., 2021. Geoscience solutions for sustainable offshore wind development. *Earth Sci. Syst. Soc.* 1 (1), 10042. <https://doi.org/10.3389/esss.2021.10042>.
- Vos, P.C., de Wolf, H., 1993. Diatoms as a tool for reconstructing sedimentary environments in coastal wetlands; methodological aspects. *Hydrobiologia (The Hague)* 269–270 (1), 285–296. <https://doi.org/10.1007/BF00028027>.
- Waajen, I.M., Busschers, F.S., Donders, T.H., van Heteren, S., Plets, R., Wallinga, J., Hennekam, R., Reichart, G.J., Kinnaird, T., Wagner-Cremer, F., 2024a. Late MIS5a in the southern North Sea: new chronostratigraphic insights from the Brown Bank Formation. *J. Quat. Sci.* 1–13. <https://doi.org/10.1002/jqs.3592>.
- Waajen, I.M., Peterse, F., Wesselingh, F.P., Busschers, F.S., Wagner-Cremer, F., van Heteren, S., Donders, T.H., 2024b. Marine and terrestrial environmental change during the MIS 5–4 transition (southern North Sea area). *J. Quat. Sci.* 39 (6), 890–904. <https://doi.org/10.1002/jqs.3647>.

- Wessex Archaeology, 2018. *Norfolk Vanguard offshore wind farm stage 3 geoarchaeological Sampling and assessment* (issue march). <https://corporate.vattenfall.co.uk/globalassets/uk/projects/norfolk-vanguard/en010079-000022-scoping-report-6.pdf>.
- Witkowski, A., Lange-Bertalot, H., Metzeltin, D., 2000. Diatom flora of marine coasts. *Iconogr. Diatomol.* 7, 1–925.
- Wolff, E.W., Chappellaz, J., Blunier, T., Rasmussen, S.O., Svensson, A., 2010. Millennial-scale variability during the last glacial: the ice core record. *Quat. Sci. Rev.* 29 (21–22), 2828–2838. <https://doi.org/10.1016/j.quascirev.2009.10.013>.
- Zagwijn, W.H., 1983. Sea-Level changes in The Netherlands during the eemian. *Geol. Mijnbouw* 62, 437–450.